9

ION SCATTERING TECHNIQUES

9.1 Rutherford Backscattering Spectrometry, RBS 476
9.2 Elastic Recoil Spectrometry, ERS 488
9.3 Medium-Energy Ion Scattering Spectrometry with Channeling and Blocking, MEISS 502
9.4 Ion Scattering Spectroscopy, ISS 514

9.0 INTRODUCTION

In this chapter three ion-scattering methods for determining composition and geometric structure (for single crystal material) are discussed. They are Rutherford Backscattering Spectrometry, RBS, which typically utilizes high-energy He or H ions (usually 1–3.4 MeV energies), Medium-Energy Ion Scattering, MEIS (ion energies from 50 keV to 400 keV), and low-energy ion scattering (100 eV to 5 keV) which is more commonly known as Ion-Scattering Spectroscopy, ISS. A fourth technique, Elastic Recoil Spectrometry, ERS, is an auxiliary to these methods for the specific detection of hydrogen. All the techniques are performed in vacuum.

For the three ion-scattering techniques there are differences in information content that are a consequence of the different ion energy regimes involved, plus some differences in instrumentation. For RBS, the most widely used method, the high-energy ions penetrate well into the sample (up to 2 μm for He ions; 20 μm for H ions). On its way into the sample an individual ion loses energy in a continuous manner through a series of electronic scattering events. Occasionally an ion undergoes a billard ball-like collision with the nucleus of an atom in the sample material and is back scattered with a discrete, large energy loss, the value of which is characteristic of the atom struck (momentum transfer). Since this major energy loss is atom specific, whereas the small continuum energy loses depend on the depth traveled, the overall energy spectrum of the emerging back scattered ions reveals both the elemental composition and the depth distribution of those elements in a nondestructive manner. Since the scattering physics is quantitatively well understood at

these high energies (Rutherford Scattering) a standardless depth profile is obtainable with a few percent accuracy. Other important factors are: the separation in backscattering energy of adjacent elements in the backscattered spectrum decreases with increasing mass such that Ni and Fe are not separable, whereas C and O are easily distinguished; the backscattering cross section is essentially proportional to $Z^2$and therefore heavy elements in light matrices have much better de- tection limits (by about a factor of 100) at 10–100 ppm than vice versa; the depth-resolution depends on ion energy, angle of incidence, and depth below the surface such that a resolution of 20 Å is achievable (low ion energy, grazing angle, analysis done right at the surface), but more typical values are several hundred angstroms.

For single crystal materials, aligning the ion beam with a crystallographic direction suppresses the signal from below the first few layers, since the atoms in these layers shadow bulk atoms below from the incoming ion beam. This technique, known as channeling, is used both to enhance the surface sensitivity and to determine the extent of crystalline defects, since if atoms are displaced from their correct positions the degree of shadowing in the channeling mode will be decreased.

MEIS is a more sophisticated form of RBS that uses lower energy ions (usually 100–400 keV) and a higher resolution ion energy analyzer. The lower energies restrict the probing depth. The better energy resolution improves the depth resolution down to a few angstroms. It also improves the ability to distinguish elements at high mass. When used for single crystal materials in conjunction with channelling of the incoming ions, and blocking of the outgoing backscattered ions, the method provides atomic positions at a surface, or an interface up to 4 or 5 layers below the surface, to an accuracy of a few hundredths of an angstrom. In addition it retains the standardless quantitation of the RBS method with sensitivities to submonolayer amounts. Both RBS and MEIS are extremely expensive, requiring an ion accelerator. The lower energy accelerator of MEIS is cheaper, but this is counteracted by the greater expense of the more sophisticated ion energy analysis. Both techniques typically cost around $1,000,000 and take up large laboratories. Beam diameters are usually millimeters in size, but microbeam systems with spatial resolution down to 1 μm exist. Ion-beam damage can be a problem, particularly for polymers. It can be mitigated by using low ion doses and by rastering the beam.

ISS involves the use of ions (usually He or Ar) in the 100–5000 eV range. At these energies essentially only backscattering from atoms in the outermost atomic layer produces peaks in the ion energy spectrum due to nearly complete neutralization of any ions scattered from below the surface. As with RBS and MEIS the ability to resolve adjacent elements becomes rapidly poorer with increasing Z. This can be mitigated, but not solved entirely, by changing the mass of the ion (eg Ar for He), the ion energy, and the angle of detection. All these variations significantly affect the scattering cross section and background, however, which complicates quantitative use. Quantitation is not standardless at these energies but requires suitable standards to determine relative cross sections for the set of scattering parame-

ters used. Cross sections still depend roughly on Z^2; however, so the technique is much more sensitive to high-Z materials. Owing to its extreme surface sensitivity ISS is usually used in conjunction with sputter profiling over the top 50 Å or so. Spatial resolution down to about 150 μm is routinely obtained. The technique is not widely used owing to the lack of commercial equipment and its poor elemental resolution. Instrumentation is quite cheap, and simple, however, since an ordinary ion gun replaces the ion accelerator used in RBS and MEIS. It can be used as an auxiliary technique on XPS or AES spectrometers by reversing the voltage on the analyzer to pass ions instead of electrons.

In ERS, also known as Forward Recoil Spectrometry, FRS, Hydrogen Recoil Spectrometry, HRS, or Hydrogen Forward Scattering, HFS, hydrogen atoms present in a sample recoil from He ions striking the sample at grazing angle with sufficient forward momentum to be ejected. They are then separated from any He that also emerges by using a thin stopping foil that allows energetic H to pass but not He. In this way the hydrogen content can be quantitatively determined. The technique can be applied in RBS, MEIS, or ISS spectrometors and is used because a target atom that is lighter than the incident ion is only scattered in the forward direction; it is never backscattered. Therefore regular RBS cannot be used for H detection. The depths analyzed and depth-profiling capabilities are similar to those of the equivalent backscattering methods, but the depth resolution is poor (~500 Å at 1000-Å depths). NRA (Chapter 11), an alternative technique for detecting hydrogen, has greater sensitivity than ERS. SIMS (Chapter 10) has far greater sensitivity for hydrogen (down to trace amounts) than either technique and better depth resolution, but it is a destructive sputter-removal method and is difficult to quantify. Sample damage can also be a problem with ERS, particularly for polymers.

9.1 RBS

Rutherford Backscattering Spectrometry

SCOTT M. BAUMANN

Contents

- Introduction
- Basic Principles
- Channeling
- Quantification
- Artifacts
- Instrumentation
- Applications
- Conclusions

Introduction

Rutherford Backscattering Spectrometry (RBS) is one of the more quantitative depth-profiling techniques available, with typical accuracies of a few percent. The depth profiling is done in a nondestructive manner, i.e., not by sputtering away the surface layers. Results obtained by RBS are insensitive to sample matrix and typically do not require the use of standards, which makes RBS the analysis of choice for depth profiling of major constituents in thin films. Detection limits range from a few parts per million (ppm) for heavy elements to a few percent for light elements. RBS depth resolution is on the order of 20–30 nm, but can be as low as 2–3 nm near the surface of a sample. Typical analysis depths are less than 2000 nm, but the use of protons, rather than helium, as the probe particle can increase the sampling depth by as much as an order of magnitude. Lateral resolution for most instruments is on the order of 1–2 millimeters, but some microbeam systems have a resolution on the order of 1–10 μm.

Three common uses of RBS analysis exist: quantitative depth profiling, areal concentration measurements (atoms/cm^2), and crystal quality and impurity lattice site analysis. Its primary application is quantitative depth profiling of semiconductor thin films and multilayered structures. It is also used to measure contaminants and to study crystal structures, also primarily in semiconductor materials. Other applications include depth profiling of polymers,[1] high-T_C superconductors, optical coatings, and catalyst particles.[2]

Recent advances in accelerator technology have reduced the cost and size of an RBS instrument to equal to or less than many other analytical instruments, and the development of dedicated RBS systems has resulted in increasing application of the technique, especially in industry, to areas of materials science, chemistry, geology, and biology, and also in the realm of particle physics. However, due to its historical segregation into physics rather than analytical chemistry, RBS still is not as readily available as some other techniques and is often overlooked as an analytical tool.

Basic Principles

RBS is based on collisions between atomic nuclei and derives its name from Lord Ernest Rutherford who first presented the concept of atoms having nuclei. When a sample is bombarded with a beam of high-energy particles, the vast majority of particles are implanted into the material and do not escape. This is because the diameter of an atomic nucleus is on the order of 10^{-4} Å while the spacing between nuclei is on the order of 1 Å. A small fraction of the incident particles do undergo a direct collision with a nucleus of one of the atoms in the upper few μm of the sample. This "collision" actually is due to the Coulombic force present between two nuclei in close proximity to each other, but can be modeled as an elastic collision using classical physics.

The energy of a backscattered particle detected at a given angle depends upon two processes: the loss of energy by the particle due to the transfer of momentum to the target atom during the backscattering event, and the loss of energy by the particle during transmission through the sample material (both before and after scattering). Figure 1 is a schematic showing backscattering events occurring at the surface of a sample and at a given depth d in the sample. For scattering at the sample's surface the only energy loss is due to momentum transfer to the target atom. The ratio of the projectile's energy after a collision to the its energy before a collision (E_1/E_0) is defined as the kinematic factor K:[3, 4]

$$K = \left(\frac{\sqrt{1 - ((M_1/M_2)\sin\theta)^2} + (M_1/M_2)\cos\theta}{1 + (M_1/M_2)} \right)^2 \tag{1}$$

where M_1 is the mass of the incident particle (typically ^{4}He); M_2 is the mass of the target atom; and R is defined as the angle between the trajectory of the He particle before and after scattering.

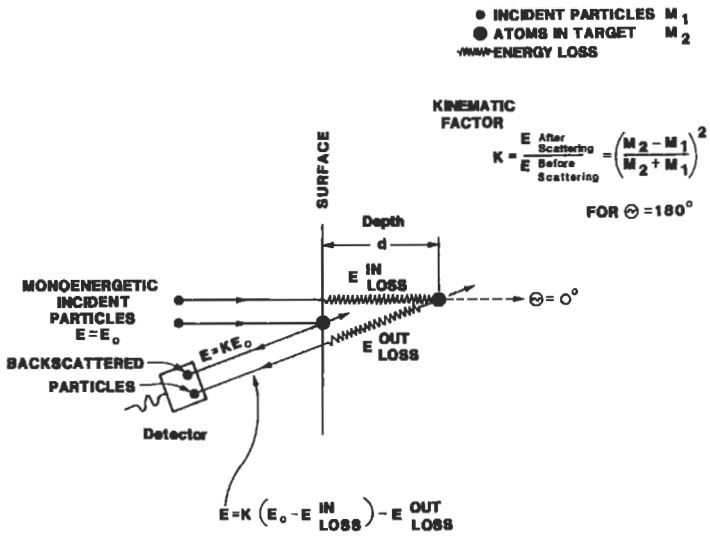

Figure 1 **A schematic showing the various energy loss processes for backscattering from a given depth in a sample. Energy is lost by momentum transfer between the probe particle and the target particle, and as the probing particle traverses the sample material both before and after scattering.**

As shown in Figure 1, when the probing particles penetrate to some depth in a sample, energy is lost in glancing collisions with the nuclei of the target atoms as well as in interactions with electrons. For a 2-MeV He atom, the energy loss is in the range of 100–800 eV/nm and depends upon the composition and density of the sample. This means that a particle that backscatters from some depth in a sample will have measurably less energy than a particle that backscatters from the same element on the sample's surface. This allows one to use RBS in determining the thickness of layers and in depth profiling.

The relative number of particles backscattered from a target atom into a given solid angle for a given number of incident particles is related to the differential scattering cross section:

$$\frac{d\sigma}{d\Omega} = \left(\frac{Z_1 Z_2 e^2}{4E}\right)^2 \frac{4\left(\sqrt{1 - \left((M_1/M_2)\sin\theta\right)^2} + \cos\theta\right)^2}{(\sin\theta)^4 \sqrt{1 - \left((M_1/M_2)\sin\theta\right)^2}} \tag{2}$$

where Z_1 and Z_2 are the atomic numbers of the incident atom and the target atom, E is the energy of the incident atom immediately before scattering, and e is the electronic charge. A rule of thumb is that the scattering cross section is basically proportional to the square of the atomic number Z of the target species. This means that RBS is more than a hundred times more sensitive for heavy elements than for light

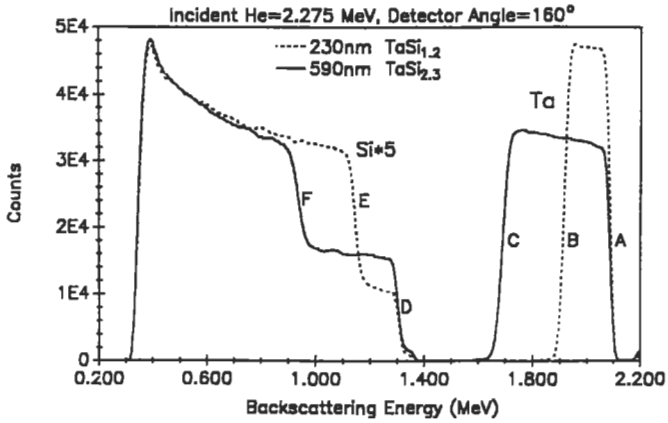

Figure 2 **RBS spectra from two $TaSi_x$ films with different Si/Ta ratios and layer thicknesses.**

elements, such as B or C. There is much greater separation between the energies of particles backscattered from light elements than from heavy elements, because a significant amount of momentum is transferred from an incident particle to a light target atom. As the mass of the target atom increases, less momentum is transferred to them and the energy of the backscattered particle asymptotically approaches the incident particle energy (see Equation 1). This means that RBS has good mass resolution for light elements, but poor mass resolution for heavy elements. For example, it is possible to resolve C from O or P from Si but it is not possible to resolve W from Ta, or Fe from Ni when these elements are present at the same depths in the sample, even though the difference in mass between the elements in each of these pairs is roughly 1 amu.

Figure 2 shows how the processes combine to create an RBS spectrum by displaying the spectra from two $TaSi_x$ films on Si substrates. Metal silicide films are commonly used as interconnects between semiconductor devices because they have lower resistivity than aluminum or polysilicon. The resistivity of the film depends upon the ratio of Si to metal and on the film thickness, both of which can be determined by RBS. The peak in each spectrum at high energy is due to scattering from Ta in the $TaSi_x$ layers while the peak at lower energy is from Si in the $TaSi_x$ layer and the Si substrate. The high-energy edge of the Ta peaks near 2.1 MeV (labeled *A*) corresponds to scattering from Ta at the surface of both samples, while the high-energy edge of the Si peaks (labeled *D*) near 1.3 MeV corresponds to backscattering from Si at the surface of the $TaSi_x$ layer. By measuring the energy width of the Ta peak or the Si step and dividing by the energy loss of He (the incident particle) per unit depth in a $TaSi_x$ matrix, the thickness of the $TaSi_x$ layer can be calculated. For example, the low-energy edge of the Ta peak corresponds to scattering from Ta at the $TaSi_x$–Si interface and the step in the Si peak corresponds to the increase in the

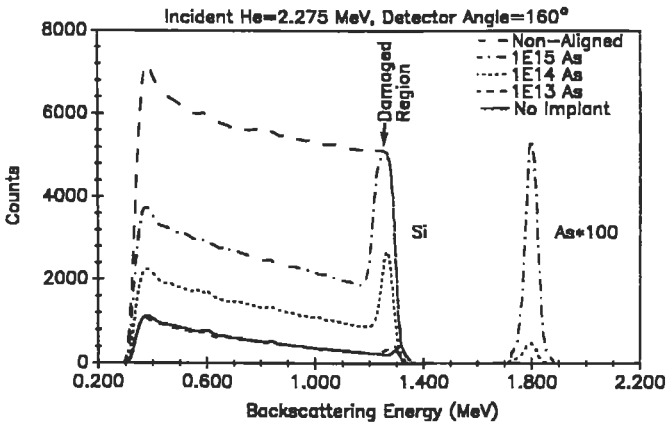

Figure 3 **Crystal channeled RBS spectra from Si samples implanted with 10^{13}, 10^{14}, and 10^{15} As atoms/cm^2. Also shown is a channeled spectrum from a nonimplanted Si sample and a nonaligned, or random, Si spectrum.**

Si concentration at the $TaSi_x$–Si interface. In this example, one of the films is 230 nm thick, while the other film is 590 nm thick. Particles scattered from Ta at the $TaSi_x$–Si interface of the 230-nm film have a final energy of about 1.9 MeV (labeled *B*) after escaping from the sample, while particles scattered from Ta at the $TaSi_x$–Si interface of the 590-nm film have a final energy of about 1.7 MeV (labeled *C*). Similarly, particles scattered from Si at the $TaSi_x$–Si interface of the 230-nm film have a final energy of about 1.1 MeV (labeled *E*) after escaping from the sample, while particles scattered from Si at the $TaSi_x$–Si interface of the 590-nm film have a final energy of about 0.9 MeV (labeled *F*). In these spectra the greater energy width of the Ta peak and the Si step for the 590-nm $TaSi_x$ film are directly related to the greater thickness of the film.

By measuring the height of the Ta and Si peaks and normalizing by the scattering cross section for the respective element, the ratio of Si to Ta can be obtained at any given depth in the film. Due to the smaller scattering cross section for Si, the Si peaks in Figure 3 have been multiplied by a factor of 5. The height of a backscattering peak for a given layer is inversely proportional to the stopping cross section for that layer, and in this case the stopping cross section of $TaSi_{2.3}$ is 1.37 times greater than that of Si. This explains why, even for the film with a Si/Ta ratio of 2.3, the height of the peak corresponding to Si in the $TaSi_x$ layer is less than ½ the height of the peak corresponding to Si in the sample substrate.

Channeling

In addition to elemental compositional information, RBS also can be used to study the structure of single-crystal samples.[5, 6] When a sample is *channeled*, the rows of atoms in the lattice are aligned parallel to the incident He ion beam. The bombard-

ing He will backscatter from the first few monolayers of material at the same rate as a nonaligned sample, but backscattering from buried atoms in the lattice will be drastically reduced, since these atoms are shielded from the incident particles by the atoms in the surface layers. For example, the backscattering signal from a single-crystal Si sample that is in channeling alignment along the (100) axis will be approximately 3% of the backscattering signal from a nonaligned crystal, or amorphous or polycrystalline Si. By measuring the reduction in backscattering when a sample is channeled it is possible to quantitatively measure and profile the crystal perfection of a sample, or to determine its crystal orientation.

Figure 3 shows channeled spectra from a series of Si samples that were implanted with 10^{13}, 10^{14}, and 10^{15} arsenic atoms/cm^2. Only the As peaks for the two highest dose implants are shown, but with a longer data acquisition time the concentration 10^{13} As atoms/cm^2 could be detected. The damage caused to the Si crystal lattice by the As implants is reflected in the peaks near 1.25 MeV in the aligned spectra. In the case of the 10^{15}-atoms/cm^2 implant there is little or no single-crystal structure remaining in the damaged region of the Si, so the backscattering signal is the same height as for nonaligned Si. Measuring the energy width of the damage peak indicates that the damaged layer is approximately 200 nm thick. Integrating the damage peak and subtracting the backscattering signal obtained for the nonimplanted reference indicates that approximately 1.0×10^{18} Si atoms/cm^2 were displaced by the 10^{15}-atoms/cm^2 As implant, while 3.4×10^{17} and 1.7×10^{16} Si atoms/cm^2 were displaced by the 10^{14}-atoms/cm^2 and 10^{13}-atoms/cm^2 As implants, respectively. In this case RBS could be used to measure accurately the total concentration of arsenic atoms implanted in each sample, to profile the As implant, to determine the amount of As that is substitutional in the Si lattice and its lattice location, to measure the number of displaced Si atoms/cm^2, and to profile the damage in the Si crystal.

Quantification

As noted above, the calculation of elemental concentrations and thicknesses by RBS depends upon the scattering cross section of the element of interest and the stopping cross section of the sample matrix. The scattering and stopping cross sections for each element have been carefully measured and tabulated.[3,4,7] In general, scattering cross sections follow the Rutherford scattering model to within 5%. It is difficult to accurately describe the stopping cross sections for all elements with a single equation, so semiempirical values are employed. A polynomial equation with several terms is used so that the stopping cross sections for each element can be calculated over a range of energies. In general, the calculated stopping cross sections are accurate to 10% or better. The stopping cross section for a multi-elemental sample is calculated by normalizing the stopping cross section of each element to its concentration in the sample.

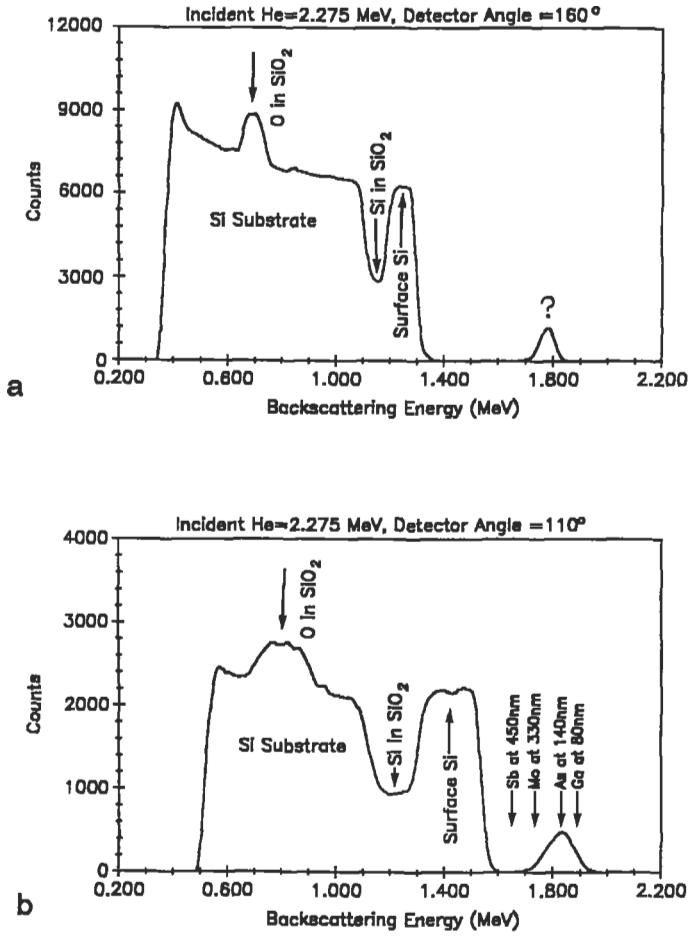

Figure 4 **RBS spectra from a sample consisting of 240 nm of Si on 170 nm of SiO_2 on a Si substrate. The spectrum in (a) was acquired using a scattering angle of 160° while the spectrum in (b) used a detector angle of 110°. This sample was implanted with 2.50×10^{16} As atoms/cm^2, but the As peak cannot be positively identified from either spectrum alone. Only As at a depth of 140 nm will produce the correct peak in both spectra.**

Due to the convoluted mass and depth scales present in an RBS spectrum, it may not be possible to accurately describe an unknown sample using a single RBS spectrum. For example, Figure 4a is an RBS spectrum acquired at a backscattering angle of 160° from a sample implanted with 2.50×10^{16} atoms/cm^2 of As at a depth of approximately 140 nm. If this were a totally unknown sample it would not be possible to determine positively the mass and depth of the implanted species from this spectrum alone, since the peak in the RBS spectrum also could have been caused by a heavier element at greater depth, such as Sb at 450 nm, or Mo at 330 nm, or by a

lighter element at a shallower depth, such as Ga at 80 nm. If an additional spectrum is acquired at a glancing backscattering angle, the scattering kinematics will be changed and the backscattered particles will have a longer escape path through the sample material to the detector. As the detector angle approaches 90° (tangent to the sample surface) the backscattering peak for a buried element will be shifted to lower energies due to the greater loss of energy along the longer escape trajectory out of the sample. Figure 4b is the RBS spectrum acquired from the same sample but at a backscattering angle of 110°. Shown in this figure are the locations for the other possible elements and depths that would match the peak shown in Figure 4a. Only As at a depth of 140 nm will produce a peak at the correct energy in both spectra. By acquiring two backscattering spectra at different angles it is usually possible to determine the depth and mass of an unknown element. One should note also that the depth resolution for the surface Si layer and the SiO_2 layer are improved in the 110° spectrum due to greater energy loss per unit depth in the sample. This results in the wider peaks for the surface Si and SiO_2 layers in the 110° spectrum.

Artifacts

Although RBS does not suffer from matrix effects that are normally associated with profiling techniques using sputtering, such as SIMS, AES, or SNMS, there are other factors that do limit the application of the technique. The convoluted nature of the mass and depth information available in an RBS spectrum often results in a spectral interference between the peak for a light element and a buried heavier element. For example, in Figure 4a the He that backscatters from the oxygen in the SiO_2 produces the peak between 0.65–0.72 MeV, while backscattering from Si in the SiO_2 produces the peak between 1.2–1.3 MeV. Scattering from the Si substrate produces the peak between 0–1.2 MeV (the backscattering signal has been suppressed between 0–0.35 MeV). The peak from the Si substrate contributes noise to the oxygen peak and limits the accuracy to which the oxygen concentration can be measured. In cases where the matrix contains heavy elements it may not be possible to detect light elements at all, i.e., carbon in a bulk tungsten sample. Procedures have been developed to eliminate or minimize the effects of these spectral interferences. These include channeling crystalline substrates to reduce the backscattering signal from the substrate, using detectors at glancing angles to the sample's surface or orienting the sample at a glancing angle to the incident ion beam, and varying the energy of the incident ion. The repeatable nature of RBS allows the use of computer models to predict the RBS spectrum from a given sample structure, permitting the investigator to optimize the measurement parameters or the sample structure to maximize the accuracy and usefulness of the results.

Sample roughness also can produce problems in the interpretation of RBS spectra that are similar to problems encountered by sputtering techniques like AES,

SIMS, and SNMS; in rare cases, such as for $HgCd_xTe_{1-x}$ samples or some polymers, the sample structure can be modified by the incident ion beam. These effects can often be eliminated or minimized by limiting the total number of particles incident on the sample, increasing the analytical area, or by cooling the sample. Also, if channeling of the ion beam occurs in a crystal sample, this must be included in the data analysis or serious inaccuracies can result. To avoid unwanted channeling, samples are often manipulated during the analysis to present an average or "random" crystal orientation.

Finally, the fundamental unit of concentration obtained by RBS is in atoms/cm^2 or concentration in the sample-versus-backscattering energy loss. To convert the profile of a backscattering peak into a depth profile it is necessary to assume a density for the material being profiled. For single-element films, such as Si, Ti, and W, an elemental density can be assumed for the film and an accurate thickness is obtained. In the case of multi-elemental films with an unknown density, a density for the film is calculated by summing the density of each element, normalized to its concentration. The accuracy of this assumption is usually within 25%, but for some cases the actual density of the film may vary by as much as 50%–100% from the assumed density. It is useful to note that:

$$T_{RBS} \times D_{RBS} = (\text{atoms})/\text{cm}^2 = D_{real} \times T_{real} \tag{3}$$

where T_{RBS} and D_{RBS} are the thickness obtained by RBS and the density assumed to calculate this thickness; and T_{real} and D_{real} are the actual physical thickness and density of the film. If the physical thickness of a film can be measured by some other technique, such as SEM, TEM, or profilometry, then the actual film density can be accurately calculated.

Instrumentation

An RBS instrument can be divided into two basic components: the particle accelerator and the analysis chamber or end station. PIXE and ERS analyses employ similar instrumentation, but use different incident ion beams or detectors.

Particle Accelerators

Two types of particle accelerators are used to obtain the MeV energies used for RBS. Single-ended accelerators are similar to ion implanters used in the semiconductor industry but have an ion source located at the high-energy terminal of the accelerator. Ions are extracted from the source and are accelerated down the beam line to ground potential. Tandem accelerators use a source that is at ground potential and that emits a beam of negative ions that are accelerated toward the positively charged terminal of the accelerator, where their charge states are changed by passing the beam through a thin foil or a gas cell. The (now) positively charged particles are accelerated to higher energy as they are repelled from the positive terminal voltage and back to ground potential.

End Station

A multitude of analysis chambers exist that have been designed with specific measurements or sample sizes in mind. State-of-the-art systems have a multiple-axis goniometer, which allows positioning of many samples for analysis without breaking vacuum. High precision (on the order of ±0.01°) is required when orienting samples for channeling, which often makes the goniometers used for channeling both complicated and expensive. The minimum sample size is controlled by the dimensions of the incident ion beam. Typically, the ion beams used for RBS are about 1–2 mm in diameter and samples are between 0.1–1 cm^2 in area, however, some microbeam systems with beam diameters on the order of 10 μm have been built. Analysis chambers also have been made to accommodate large samples, such as entire silicon wafers. For the purposes of most standard RBS measurements the analysis chamber needs to be evacuated to at least 10^{-5} torr. Extremely good depth resolutions of less than 3 nm can be obtained by orienting either the incident ion beam or rhe detector at a glancing angle to the sample surface.

Applications

Listed below is a summary of some common applications of RBS.

Semiconductors:	Quantitative depth profiling of: Metal silicide films (WSi_x, $MoSi_x$, $TiSi_x$, etc.) Barrier metals (TiN_x, TiW_x, etc.) Insulating layers (SiO_x, SiN_x, and SiO_xP_y) Cu in Al interconnect III-V and II-VI materials ($Al_xGa_{1-x}As$, and $Hg_xCd_{1-x}Te$) Metal multilayer stacks Dose/lattice substitutionality of implanted species Crystal damage versus depth (Si, $SiGe_x$, $Al_xGa_{1-x}As$, and $Hg_xCd_{1-x}Te$)
High-T_C superconductors:	Quantitative depth profiling ($YBa_xCu_yO_z$, and $BiSr_wCu_xCa_yO_z$) Crystal orientation and damage versus depth
Optical/antireflective coatings:	Quantitative depth profiling of multilayered stacks (SiO_2, HfO_2, TiO_2, SnO_2, $InSn_xO_y$, etc.)
Polymers:	Depth profiling of halogens and impurities Metallization of surfaces
Catalysts:	Location of active ions on or in particles

Conclusions

RBS is a rapidly growing technique that has evolved from being used primarily in particle physics to being commonly applied and widely available. The size and cost of some RBS instruments are now equal to or less than that of other depth profiling techniques, such as SIMS, AES, and SNMS. RBS data analysis software allows most data to be rapidly and accurately analyzed and permits the automated acquisition of and (in some cases) analysis of data. Currently RBS is used primarily in the analysis of semiconductors, superconductors, optical coatings, and other thin films. Some applications have been developed for polymers and ceramics, and further growth is expected in these areas due to the technique's relatively lenient vacuum requirements and its insensitivity to charging problems for insulators. A few microbeam RBS systems are currently in service and the development of RBS imaging will certainly produce new applications for semiconductors and, possibly, even for biological samples, since the small size of cells that are typically analyzed has limited the use of RBS in the past.

Related Articles in the Encyclopedia

MEIS, ISS, PIXE, ERS, and NRA

References

1 S. J. Valenty, J. J. Chera, G. A. Smith, W. Katz, R. Argani, and H. Bakhru. *J. Polymer Sci. (Chem.)* **22,** 3367, 1984.

2 S. M. Baumann, M. D. Strathman, and S. L. Suib. *Analytical Chem.* **60,** 1046, 1988.

3 W. K. Chu, J. W. Mayer, and M. A. Nicolet. *Backscattering Spectrometry.* Academic Press, New York, 1978. This is a frequently used handbook that provides a thorough discussion of the technique.

4 J. R. Bird and J. S. Williams. *Ion Beams for Materials Analysis.* Academic Press, Australia, 1989. Chapter 3 provides an overview of RBS, while Chapter 6 reviews channeling techniques. This book also reviews NRA, PIXE, SIMS, and other related ion-beam analyses.

5 L. C. Feldman, J. W. Mayer, and S. T. Picraux. *Materials Analysis by Ion Channeling.* Academic Press, New York, 1982. This book provides an in-depth study of the principles and use of ion channeling for analyzing materials.

6 *Channeling.* (D. V. Morgan, ed.) John Wiley & Sons, London, 1973. Chapters 13–16 provide information regarding the use of channeling

measurements in the analysis of materials. The remainder of the book is a study of the physics of channeling.

7 J. F. Ziegler, J. P. Biersack, and U. Littmark. *Stopping Powers and Ranges in All Elements.* Pergamon Press, New York, 1977, vol.1-6.

8 D. K. Sadana, M. Strathman, J. Washburn, and G. R. Booker. *App. Phys. Letts.* **37,** 234, 1980.

9 *Ion Beam Handbook for Material Analysis.* (J. W. Mayer and E. Rimini, eds.) Academic Press, New York, 1977. This book provides useful tabular and graphic data for RBS, channeling, PIXE, and NRA.

9.2 ERS

Elastic Recoil Spectrometry

J.E.E. BAGLIN

Contents

- Introduction
- Principles of ERS
- Practical Considerations
- Conclusions

Introduction

Overview

Elastic recoil spectrometry (ERS) is used for the specific detection of hydrogen (^{1}H, ^{2}H) in surface layers of thickness up to approximately 1 μm, and the determination of the concentration profile for each species as a function of depth below the sample's surface.[1, 2] When carefully used, the technique is nondestructive, absolute, fast, and independent of the host matrix and its chemical bonding structure. Although it requires an accelerator source of MeV helium ions, the instrumentation is simple and the data interpretation is straightforward.

The method may be contrasted to dynamic SIMS analysis, which, although capable of somewhat better depth resolution, is slower and matrix-dependent, and relies on ion milling (sputtering) for profiling. Nuclear Resonance Reaction Analysis (NRA) claims, in general, a better ability to identify trace (ppm) hydrogen levels, mainly because of enhanced (resonant) scattering cross sections. However, a depth profile determination by NRA is complex, requiring many sequential data runs, and it takes many times longer than ERS. Quantitative NRA data reduction is

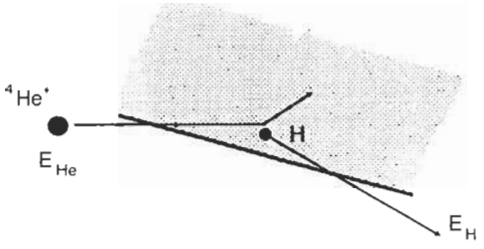

Figure 1 **The forward scattering concept of ERS.**

hampered by the difficulties of determining and deconvoluting the nuclear resonance shapes.

ERS may be regarded as an extension of Rutherford Backscattering Spectrometry (RBS).[3] It requires basically identical equipment, and it preserves many beneficial features of RBS: convenience, speed, precision, and simplicity. RBS is based on the simple point-charge scattering of ions (generally helium at 1–2 MeV) by the constituent atomic nuclei of the sample. The energy of ions scattered at a known angle is used to indicate both the mass of the scattering nucleus and the depth of penetration of the ion into the sample before the scattering collision occurred. To optimize mass resolution and sensitivity, those ions which are scattered backwards (near 180°) are frequently chosen for RBS spectrometry. This geometry does not work, however, when the projectile is heavier than the target nucleus. As illustrated in Figure 1, following the collision of a helium ion with a hydrogen (or deuterium) nucleus in the sample, both particles move in the forward direction, and it is therefore necessary to place detectors to receive forward scattered particles. Since most specimens will be too thick to allow either ^{4}He or H ions to escape in transmission geometry, a glancing angle arrangement is chosen. In this situation, it is advantageous to select the recoiling hydrogen ions themselves for energy spectrometry, rather than the lower energy, less-penetrating scattered helium ions. By covering the detector with a stopping foil of appropriate thickness, it is possible to admit H ions for analysis but exclude all scattered He ions, including the prolific He ion flux contributed by Rutherford scattering from other, heavier constituents of the sample.

The covered detector thus provides an energy spectrum of the forward-recoiling hydrogen ions. An important advantage of this technique is the uncomplicated relationship between this spectrum and the concentration-versus-depth profile for hydrogen in the sample. Derivation of the concentration profile is direct and unambiguous. This simplicity depends on the He–H scattering process being elastic (no residual excited states of scattered nuclei), and on the absence of nuclear reactions that might yield spurious detectable particles. The threshold energies for

such reactions are 6.7 MeV (for $^4He + {}^2H \rightarrow {}^4He + n + p$), and tens of MeV for ^1H. Typically, ERS measurements are run with 1–2 MeV ^4He ions, where such problems do not arise.

Although most applications of ERS have used ^4He as the projectile ion, the principle clearly can be extended to recoiling ions from heavier projectiles. The depth resolution may be significantly improved in this way, e.g., in polystyrene, the resolution found[4] for ERS from 2.8-MeV He ions was 1000 Å, compared with 300 Å obtained by using 20-MeV Si ions. Also, the scattering cross section is larger for Si, leading to greater sensitivity. Severe radiation damage to samples can occur with heavy ions, however (factors of >100 worse than for He). In the interest of simplicity, this review will focus on the technique of hydrogen detection using helium ion beams.

Applications

ERS is an appropriate tool for a wide range of analytical applications. Some typical examples include the quantitation of hydrogen in glassy carbon films, the study of the dynamics of polymeric molecules,[5] studies of interface interactions between polymer films (using deuterium as a diffusion marker),[4] analysis for hydrogen in natural geological specimens,[6] a study of stress-induced redistribution of hydrogen in metal films,[7] and a study of the effects of hydrogen content upon the optical, mechanical, and structural properties of plasma-deposited amorphous silicon and silicon nitride films.[8,9] Further applications will also be found in the specific examples cited in this article.

Principles of ERS

Apparatus

A typical experimental equipment layout for ERS is shown schematically in Figure 2. A beam of ^4He ions is produced at an energy of 1–2 MeV, generally using an electrostatic accelerator and a beam transport system including a mass- and energy-resolving bending magnet and knife edge collimators to define the beam spot size and position. A typical beam current required is 5–50 nA, with a beam spot dimension of 1–2 mm. A clean vacuum of $\leq 10^{-7}$ Torr is desirable for particle spectrometry, and specimens must be vacuum compatible. The specimen is tilted so that the incident beam makes an angle of approximately 15° with the plane of the surface, and a surface barrier detector is placed to receive particles scattered at a similar angle from the sample surface in the forward direction. The detector's aperture is set to limit the range of accepted scattering angles to $\pm 1°$ or less. A smooth foil of aluminum or Mylar is placed in front of the detector to stop scattered He ions, yet to transmit scattered ^1H (or ^2H) ions into the detector after they incur a small, well-defined energy loss. It is important for this foil to be uniform and free of

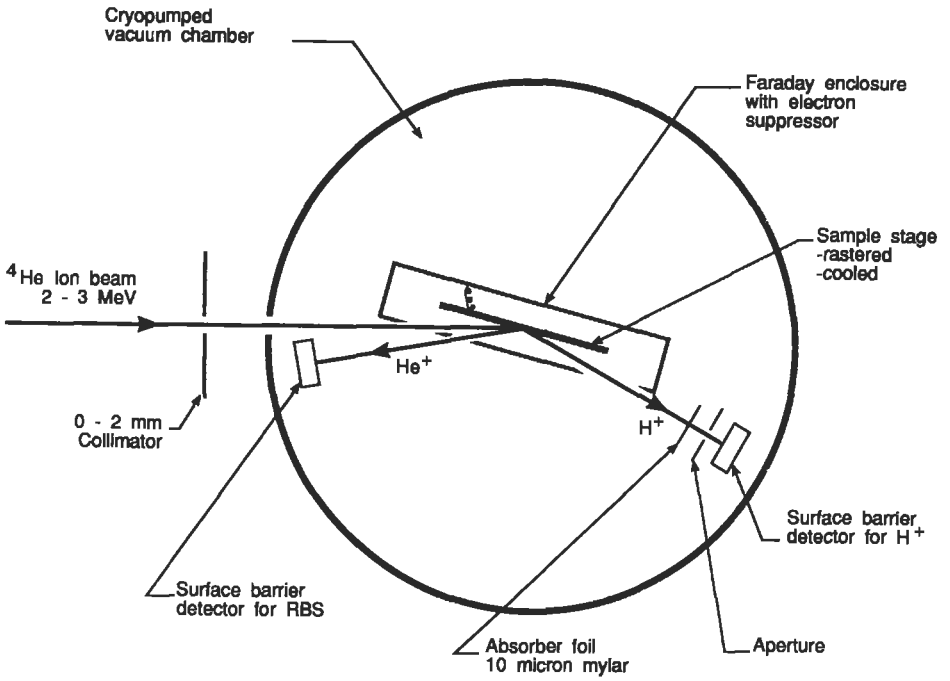

Figure 2 **Typical experimental layout for ERS (schematic).**

pinholes. A 10-μm Mylar foil will completely stop He ions of energy ≤ 2.3 MeV, while transmitting recoiling ^{1}H ions with an energy loss of 250 keV. An energy spread of ≤ 50 keV in the transmitted ions will be caused by straggling.[3] A second surface barrier detector normally is used in a backscattering position. Spectra accumulated simultaneously with this detector will provide RBS information on the sample's composition which must be combined with the ERS data for a complete sample analysis. Quantitative analysis requires a reliable measure of the incident ion fluence for each run. As in RBS, this may be obtained in various ways, either by direct collection of ion beam charge on the sample and in a surrounding Faraday enclosure (as illustrated in Figure 2), or by a well calibrated beam current sampling technique. In the former technique, complete collection of secondary electrons from the sample surface must be assured. A cooled sample stage mounted on a goniometer provides the means to adjust the sample's orientation and, ideally, to raster the sample, in order to limit local ion beam heating. The sample stage may be cooled with liquid nitrogen to reduce the effects of beam-induced damage on the analysis, especially for polymers. Signals from the two surface barrier detectors are sorted by a pulse height analyzer, and the resulting spectra are stored for subsequent display and quantitative analysis. Typical run times of 15–20 minutes are required to obtain good statistics. It should be noted that this technique responds exclusively

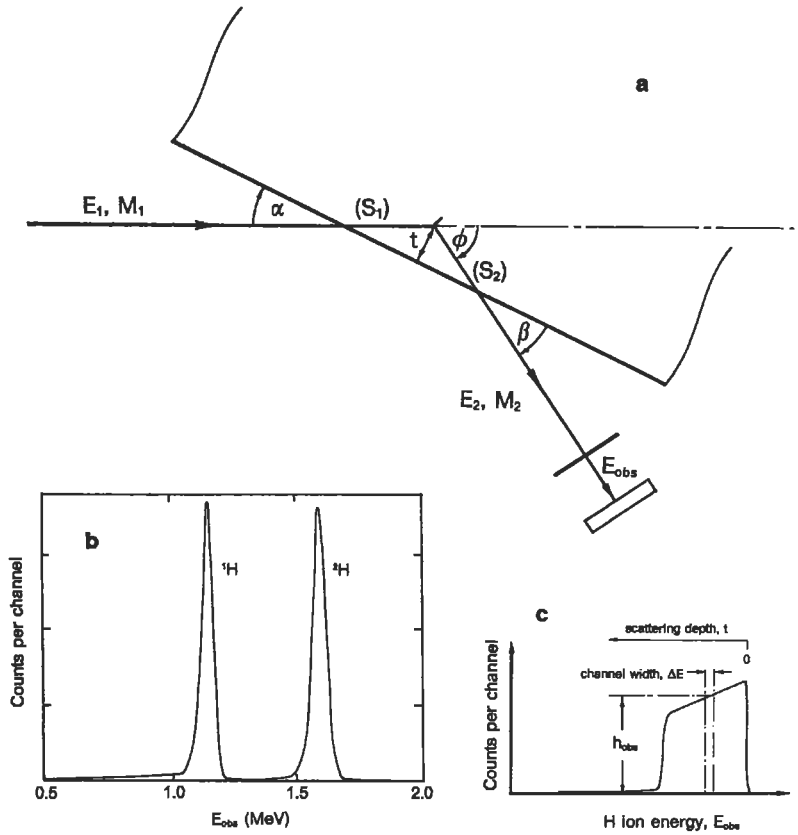

Figure 3 **(a) Scattering geometry for ERS; (b) ERS spectrum from 200-Å partially deuterated polystyrene on Si, E_1 = 3.0 MeV (adapted from ref. 10); and (c) schematic ERS depth profile spectrum.**

to the presence of ^1H or ^2H (or ^3H or ^3He) nuclei in a sample, and does not suffer from any "background" from other sources. The sensitivity of the technique to trace amounts of H is therefore largely determined by patience and counting statistics.

Energy Scale of ERS

The energy scale of an elastic recoil spectrum provides information about the mass of the recoiling species, and about the depth within a sample at which the scattering took place.

Figure 3a shows the ERS scattering geometry. To generalize the treatment, the following identities are adopted: ϕ is the angle of hydrogen recoil with respect to the incident beam; M_1 and E_1 are the mass and energy, respectively, of the incident ion; M_2 is the mass of the recoiling ion; E_2 is the energy of the recoiling particle at the point of the collision.

For the simple case of surface scattering (or scattering from a very thin layer), the ratio of E_2 to E_1 is given by

$$\frac{E_2}{E_1} = \frac{4M_1M_2\cos^2\phi}{(M_1+M_2)^2} \tag{1}$$

This ratio is known as the kinematic factor K'. The separation obtainable between ^{1}H and ^{2}H is evident ($K'(^1\text{H}) = 0.64\cos^2\phi$; $K'(^2\text{H}) = 0.88\cos^2\phi$), as seen in the energy spectrum of detected particles shown in Figure 3b, which was obtained from a 200-Å film of deuterated polystyrene on a silicon substrate.[10] In practice, ϕ is generally set in the range of 10–30°.

When a stopper foil of thickness δ_f(atom/ cm^2) is used, the hydrogen energy observed at the detector is not actually E_2, but a lower value, E_{obs}, where

$$E_{obs} = E_2 - \delta_f S_f \tag{2}$$

where S_f is the "stopping power" for hydrogen ions in the foil at the appropriate energy; i.e., the energy lost per unit thickness (atom/ cm^2) of foil material. Obviously, it is best to choose the smallest δ_f consistent with total stopping of unwanted ^{4}He ions.

In the more complex situation, a helium ion penetrates to a depth t (normal to the surface) into the sample before encountering a hydrogen nucleus, where scattering occurs. The helium ion loses energy in ionizing collisions before the scattering event, and in turn the recoiling H must undergo a similar energy loss before escaping the sample's surface. If the energy-averaged stopping powers for ^{4}He and recoiling H within the sample are S_1 and S_2, respectively, then the depth t of the recoiling collision may be derived from the expression[11]

$$t = (E_{obs} + \delta_f S_f - K'E_1)\left(\frac{K'S_1}{\sin\alpha} + \frac{S_2}{\sin\beta}\right)^{-1} \tag{3}$$

Generally $S_2 << S_1$. In this way, a depth scale may be associated with an ERS spectrum, as shown in the schematic spectrum of Figure 3c. That spectrum shows the H recoil rate (counts per energy channel of width ΔE) as a function of E_{obs} and hence as a function of depth below the sample surface (see Equation (3)).

Total Hydrogen Content

As with RBS, the simplest and most precise measurement that ERS can provide is the absolute measure of total hydrogen content (^{1}H and/or ^{2}H) within a surface layer or film of thickness less than a few thousand angstroms. When the layer is thin, this is determined from the total number of events, or *yield* Y summed over the elastic recoil spectral peak. The yield may be expressed as

$$Y(E_1, \phi) = \frac{d\sigma}{d\Omega}(E_1, \phi) \cdot Q \cdot \Omega \cdot N_H \tag{4}$$

where $d\sigma/d\Omega$ (E_1, ϕ) is the differential cross section for the nuclear scattering process ^{x}H(^{4}He,^{x}H)^{4}He; Q is the total number of ^{4}He ions striking the sample (integral charge ÷ $q_{electron}$); Ω is the solid angle subtended by the recoil detector at the sample; and N_H is the density (atoms/cm^2) of ^{x}H in the layer. The quantities Q, Ω, and Y may be readily and precisely measured. Hence N_H may be derived provided that $d\sigma/d\Omega$ is precisely known.

Cross Section $d\sigma/d\Omega$ (E_1, ϕ)

In the analogous RBS analysis, $d\sigma/d\Omega$ is given precisely and analytically by the Rutherford scattering formula. Unfortunately, the case of (^{4}He, ^{x}H) scattering is not quite so simple. While the processes are indeed elastic, their cross sections are dominated by nuclear interaction components except at very low energies. (The ^{1}H(^{4}He, ^{1}H)^{4}He cross section approaches the Rutherford value for energies below 0.8 MeV.)

The absolute precision of ERS therefore depends on that of $d\sigma/d\Omega$ (E_1, ϕ). Unfortunately, some disagreement prevails among measurements of the ^{1}H recoil cross section. One recent determination[6] is shown in Figure 4a for $\phi = 30°$ and 25°. The convergence of these data with the Rutherford cross section near 1 MeV lends support to their validity. The solid lines are least squares fits to the polynomial form used by Tirira et al.[6]. For $\phi = 30°$, the expression reads:

$$\ln \frac{d\sigma}{d\Omega} = 0.133\,E_1 + 4.383 + 2.196\,(1.6454)\,E_1^{-1} - 0.042\,E_1^{-2} \tag{5}$$

where E_1 is expressed in MeV and the cross section in units of 10^{-27} cm^2/sr. Such an expression is of practical value for computer evaluation of measured spectra.

The measured cross section data for ^{2}H are shown[12] in Figure 4b. The dominant resonance at 2.13 MeV offers a powerful enhancement to sensitivity for deuterium detection, exceeding the Rutherford cross section by two orders of magnitude.

Concentration Profiles

As in RBS analysis, ERS can provide information on the atomic concentration of hydrogen as a function of depth (measured in atoms/cm^2). This is derived from the "height" h_{obs} of the ERS spectrum (counts per channel), at energies corresponding to particular depths within the sample (see Figure 3c). For a sample consisting of H and another material X, with composition H_mX_{1-m}, the spectrum height h_{obs} may be expressed

$$h_{obs} = \frac{m \cdot \dfrac{d\sigma}{d\Omega} \cdot Q \cdot \Omega \cdot \Delta E}{[S]^{H_mX_{1-m}} \cdot \sin\alpha} \left(1 - \delta \frac{dS_f}{dE}\right)^{-1} \tag{6}$$

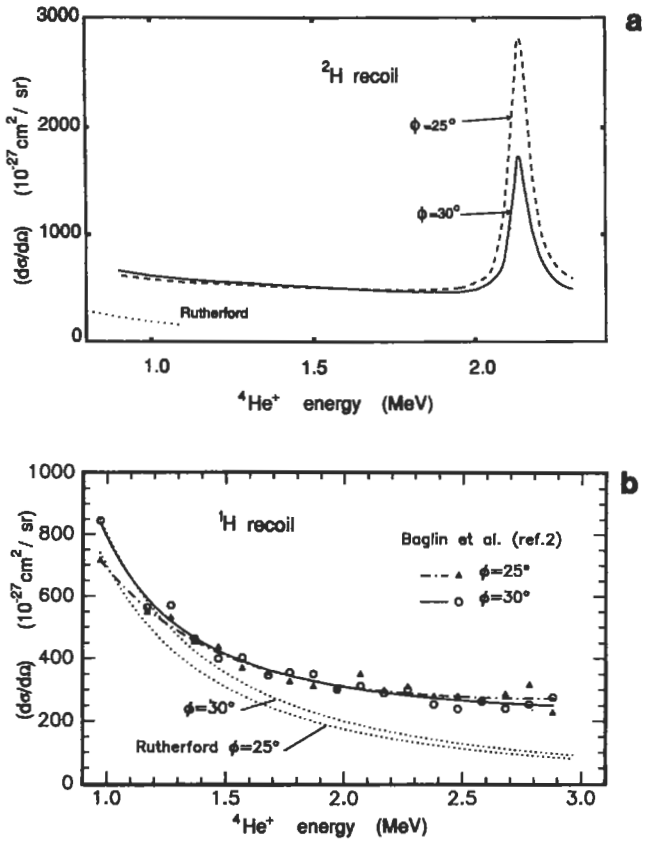

Figure 4 **(a) Differential cross section data for ^{1}H (^{4}He, ^{1}H) ^{4}He scattering at $\phi \equiv 30°$ and 25°; and (b) differential cross section data for ^{2}H (^{4}He, ^{2}H) ^{4}He scattering measured at ϕ = 30° and 25° (adapted from ref. 12). The dotted lines locate the Rutherford scattering cross sections for comparison.**

where $[S]$ is a *reduced stopping power* serving to combine the effects of energy losses within the sample, given by the expression

$$[S]^{\mathrm{H}_m X_{1-m}} = \frac{K'}{\sin\alpha} \cdot [S]^{\mathrm{H}_m X_{1-m}}_{\mathrm{He}} + \frac{1}{\sin\beta} \cdot [S]^{\mathrm{H}_m X_{1-m}}_{\mathrm{H}} \tag{7}$$

In turn, the stopping powers $[S]_{\mathrm{He}}$ and $[S]_{\mathrm{H}}$ are obtained by the application of Bragg's rule to combine the stopping powers in H and in *X*:

$$[S]^{\mathrm{H}_m X_{1-m}}_{\mathrm{He}} = m \cdot [S]^{\mathrm{H}}_{\mathrm{He}} + (1-m) \cdot [S]^{X}_{\mathrm{He}} \tag{8}$$

The final term of Equation (6) corrects for the distortion of the ERS spectrum caused by velocity-dependent energy losses as the H ions pass through the stopper foil.

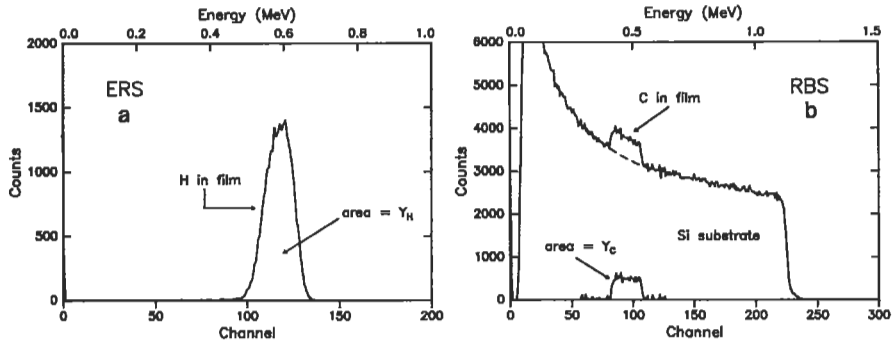

Figure 5 **ERS and RBS spectra for a 1000-Å sputter-deposited diamond-like carbon film on Si. Both spectra are required for complete analysis.**

The value of m may thus be derived from the spectrum height h_{obs} at an energy E_{obs}, whose value indicates the depth of the layer described. The precision of this measurement will be limited by the precision of $(d\sigma/d\Omega)$ and by the precision of stopping powers. Values of elemental stopping powers are available from compilations of experimental data that have been cross correlated for Z systematics.[13] Nevertheless, these stopping powers are still not well established, and their uncertainty may reach 10 % or more. The spectrum height therefore offers limited precision for direct measurement of m. However, the dependence of m upon depth can generally be accurately deduced from the energy dependence of h_{obs}.

Combined ERS and RBS Data

The use of RBS concurrently with ERS is necessary for the complete derivation of a hydrogen profile, and it offers some simplifications of analysis. For example, for thin-layer spectra that have been normalized for a common ion fluence Q and solid angle Ω, the total yields Y (the areas under the spectral peaks) may be compared in order to derive the layer composition. For H_mX_{1-m},

$$\frac{m}{1-m} = Y_H \cdot \left(\frac{d\sigma}{d\Omega}\right)^{-1}_{ERS} \cdot \left(\frac{d\sigma}{d\Omega}\right)_{RBS} \cdot \frac{1}{Y_X} \tag{9}$$

where Y_H, Y_X are the areas for the H component in the ERS spectrum and for the X component in the RBS spectrum, respectively. Figure 5 illustrates such a measurement for a sputter-deposited diamond-like carbon film on a silicon substrate. Taking the areas of the peaks shown (normalized by the respective detector solid angles), and values of $d\sigma/d\Omega$ from Figure 4, and substituting in Equation (9) leads to the composition $H_{30}C_{70}$ in this case.

Similarly, it is possible to derive an expression relating the ratio of spectral heights h_{RBS} found for one or more elements in the RBS spectrum with that

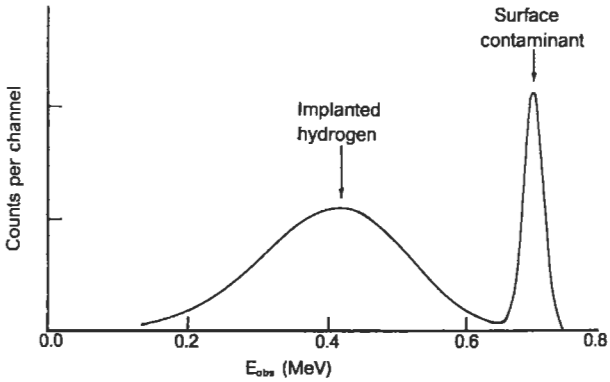

Figure 6 **Computer-simulated ERS spectrum (adapted from ref. 6) for the case of 1.6-MeV ^{4}He probing a silicon wafer implanted with 0.9×10^{16} H atoms/cm^2 at 10 keV (mean range of ions = 1750 Å, $\phi = 20°$, $\alpha = 10°$).**

obtained for hydrogen, h_{obs}, in the corresponding ERS spectrum. In this case, all data must correspond to a layer at a common depth in the sample. Since the RBS geometry differs from that of ERS, the RBS equivalents of Equation (6) must be derived. The resulting expression for h_{obs}/h_{RBS} may be used to calculate the sample composition at that depth.

Spectrum Simulation and Fitting

In the absence of a simple deconvolution procedure, an effective tool for determining a composition profile for a multilayered hydrogen-containing system is the simultaneous empirical fitting of observed ERS and RBS spectra with those calculated layer-by-layer for a trial sample structure. This requires straightforward software and data bases for $d\sigma/d\Omega$ and S, similar to those used for RBS fitting by RUMP and other standard packages. An example of such a computed ERS spectrum[6] is shown in Figure 6. The principal (broad) peak represents the expected distribution of ^{1}H (0.9×10^{16} atoms/cm^2) implanted in silicon at 10 keV (mean depth 1750 Å, range spread ± 700 Å), while the narrow peak corresponds to a surface contaminant layer. The simulated spectrum is an excellent fit to the corresponding experimental data.[6]

Heavy Ion Scattering

ERS can be applied to analysis for light elements other than hydrogen; the primary requirements are that the bombarding ion should be much heavier than the recoiling species being detected, and that inelastic nuclear reactions should not dominate; scattering cross sections must be known or determined; the spectrometer must be suitable for detecting recoiling species more massive than hydrogen; for depth profiling, greater ion energies are required, in general, increasing the risk of sample damage.

Practical Considerations

Sample Damage

High-energy He ions readily produce atomic displacements and broken chemical bonds in solids. While in many inorganic materials, the disordering is negligible during a 2-MeV He exposure for RBS, the situation for hydrogen is particularly sensitive. The probing He beam can readily liberate hydrogen from the near-surface regions of metal hydrides, and can cause substantial dissociation of polymers with concurrent loss of hydrogen from the sample. Special precautions must always be taken to minimize or quantify this effect, so that ERS will not alter the sample during analysis.

An example of the effect is the case of a 1000-Å polystyrene film deposited on a silicon wafer, which was subjected to successive exposures of 10 μC of helium ions, at room temperature (beam current 10 nA; sample area 4 mm^2). Each run produced ~1 % depletion in hydrogen content, while RBS showed no loss of carbon. The loss was shown to depend on cumulative ion fluence, rather than on beam current density. The sample analysis can be corrected for hydrogen loss by extrapolating to zero exposure. In general, for large beam current densities, thermal effects can become significant (depending on the nature of the polymer itself), increasing the loss rate of volatile hydrocarbons generated by radiation damage. In such cases, the use of a broadly rastered sample area and sample cooling may be helpful.

A further damage problem can be presented by thick samples of highly nonconducting material (e.g., ceramics), within which the incoming ion beam can build up electrostatic charge to the point of plasma discharge. Fracture or dissociation within the sample can result, and hydrogen (or other constituents) may well be liberated from the sample. The problem may be reduced with the use of conducting coatings and low beam current densities.

Reference Samples

Susceptibility to radiation damage must be considered seriously if reference samples are to be calibrated for use in place of absolute systems. For the measurement of absolute (^4He, ^1H) cross sections, films of polystyrene $(CH)_n$ (which is relatively radiation hard) have been used successfully, the RBS determination of carbon providing implied quantitation for the hydrogen present in the film. For a durable laboratory reference sample, however, there is much to recommend a known ion-implanted dose of H deep within Si or SiC, where the loss of hydrogen under room temperature irradiation will be negligible.

Depth Resolution

The depth resolution of ERS is typically found to be in the 300–600 Å region (at a depth of 1000 Å in silicon), which is not as good as one might wish for interface

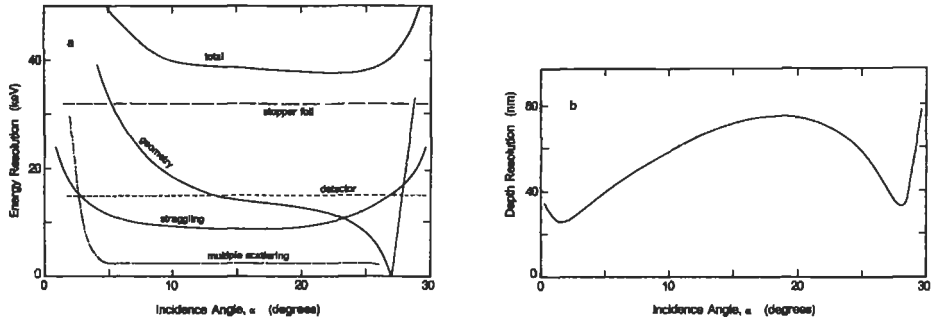

Figure 7 **(a) Major depth resolution contributions from experimental factors in ERS, as functions of sample tilt angle α, assuming $\phi = 30°$; and (b) net depth resolution calculated at a depth of 1000 Å in Si, as a function of α (adapted from ref. 14).**

and thin-film structure studies. The need to select analysis geometry and detectors that optimize resolution for a given situation must be stressed.

Figure 7a displays, for H at a depth of 1000 Å in silicon, the major contributions[14] to spectral energy resolution loss in a typical ERS configuration (recoil angle $\phi = 30°$), and their dependence on the sample tilt angle α.

Hydrogen ion energy straggling in the thick stopper foil is a large contribution. Care must be exercised to see that the foil does not contribute even more due to irregularities or pinholes. Otherwise, the only recourse is to replace the foil and detector with a cumbersome and costly electrostatic, magnetic, or time-of-flight spectrometer. This also could overcome some of the inherent limitations on the energy resolution of surface barrier detectors. It is worth noting that, due to the $\cos^2\phi$ dependence of K', the detector's aperture must limit its acceptance angle, $\Delta\phi$ to about 1°, to reduce geometrical degradation of resolution.

Figure 7 shows a contribution from ion energy straggling[3] in the sample. This, of course, is zero for near-surface layers and gets rapidly worse for layers several thousand Å deep, or for (α, ϕ) in grazing configurations.

The curve labeled *geometry* illustrates the kinematic energy spread due to the finite acceptance angle of the detector. The multiple scattering contribution arises from the spread in ion energies introduced by secondary scattering events.

Figure 7b shows the physical depth resolution resulting from the energy resolution of Figure 7a. Evidently, depth resolutions for H in silicon, using $\phi = 30°$, would be optimized by selecting a grazing geometry (α or $\beta \approx 2°$). Such a geometry presents practical problems, however. A more fruitful approach may be to accept the more convenient geometry ($\alpha = \beta$) and to control depth resolution by replacing the foil-covered detector with a magnetic spectrometer, thereby removing the largest contributor to resolution broadening.

Enhanced depth resolution could be obtained by using high-energy heavy ions (e.g., 20-MeV ^{28}Si) in place of ^{4}He, due to their higher stopping power in the sample.[4] Radiation damage problems then are much greater, however, and also a high-energy accelerator is required.

Conclusions

ERS constitutes a powerful, fast, and quantitative technique for depth profiling of hydrogen and deuterium in solids. The method is very appropriate, convenient, and fast for the quantitation of ^{1}H and ^{2}H in thin films or surface layers, in which total recoil counts lead directly to the hydrogen content in atoms/cm.[2] The result is free of solid-matrix effects, which can dominate lower energy techniques like SIMS. Its sensitivity to small amounts of hydrogen is high, and its natural identification of ^{1}H and ^{2}H makes deuterium tracer experiments easy. The depth resolution of ERS within a solid is not as good as that of SIMS, due mainly to the effect of the stopping foil and the energy resolution limits of surface barrier detectors. However, excellent concentration profiles have been obtained. While ERS is applicable in all materials that are vacuum compatible, radiation damage of samples can affect the results, especially in polymers or unstable hydrides; this problem usually can be overcome by sample rastering. ERS is easy to run concurrently with RBS, since identical apparatus is used. Such complementary runs provide a ready means for complete elemental analysis of hydrogen-containing thin film samples.

ERS is still being developed, refined, and enhanced to improve its depth resolution and absolute precision, to facilitate data reduction and to minimize sample damage. Excellent results can be achieved simply by implementing ERS with careful regard for the issues described in this article.

Related Articles in the Encyclopedia

RBS, NRA, and SIMS

References

1 J. L'Ecuyer, C. Brassard, C. Cardinal, and B. Terrault. *Nucl. Instr. and Methods.* **149,** 127, 1978.

2 B. L. Doyle and P. S. Peercy. *Appl. Phys. Lett.* **34,** 811, 1979.

3 W.-K. Chu, J. W. Mayer, and M. A. Nicolet. *Backscattering Spectrometry.* Academic Press, New York, 1978.

4 P. F. Green and B. L. Doyle. Hydrogen and Deuterium Profiling in Polymers using Light and Heavy Ion Elastic Recoil Detection. In *High Energy and Heavy Ion Beams in Materials Analysis.* (J. R. Tesmer, C. J. Maggiore, M. Nastasi, J. C. Barbour, and J. W. Mayer, eds.) Materials Research Society, Pittsburgh, 1990.

5 P. F. Green and E. J. Kramer. *J. Mat. Res.* **1,** 202, 1986.

6 J. E. E. Baglin, A. J. Kellock, M.A. Crockett and A. H. Shih, *Nucl. Instr. and Methods* **B64**, 469, 1992; see also J. Tirira, P. Trocellier, J. P. Frontier, and P. Trouslard. *Nucl. Instr. and Methods.* **B45,** 203, 1990.

7 L. S. Wielunski, R. E. Benenson, and W. A. Lanford. *Nucl. Instr. and Methods.* **218,** 120, 1983.

8 H. Cheng, Z.-Y. Zhou, F.-C. Yang, Z.-W. Xu, and Y.-H. Ren. *Nucl. Instr. and Methods.* **218,** 601, 1983.

9 M. F. C. Willemsen, A. E. T. Kuiper, L. J. van Ijzendoorn, and B. Faatz. ERD in IC Related Research. In *High Energy and Heavy Ion Beams in Materials Analysis. op cit.*

10 L. C. Feldman and J. W. Mayer. In *Fundamentals of Surface and Thin Film Analysis.* North Holland, New York, 1986, p. 61.

11 J. E. E. Baglin and J. S. Williams. High Energy Ion Scattering Spectrometry. In *Ion Beams for Materials Analysis.* (J. R. Bird and J. S. Williams, eds.) Academic Press, Sydney, 1989.

12 F. Besenbacher, I. Stensgaard, and P. Vase. *Nucl. Instr. and Methods.* **B15,** 459, 1986.

13 J. F. Ziegler. *The Stopping Power and Ranges of Ions in Matter.* Pergamon Press, New York, 1977, vols. 3 and 4.

14 A. Turos and O. Meyer. *Nucl. Instr. and Methods.* **B4,** 92, 1984.

9.3 MEIS

Medium-Energy Ion Scattering Spectrometry with Channeling and Blocking

T. GUSTAFSSON AND P. FENTER

Contents

- Introduction
- Basic Principles
- Instrumentation
- Examples and Applications
- Conclusions

Introduction

Medium-Energy Ion Scattering (MEIS) with channeling and blocking is a quantitative, real-space, nondestructive technique for studying the composition and structure of surfaces and buried interfaces. "Medium" energy is roughly the energy region between 50 keV and 300 keV. This region is sufficiently high so that the ion–surface interaction law is simple and well characterized—essentially only classical Rutherford scattering is involved—and sufficiently low so that the surface specificity is optimized. The basic quantities measured are the energy and angular distribution of backscattered ions. The technique derives elemental specificity from the fact that the energy of a backscattered ion is a strong function of the mass of the target atom. As the ions propagate through the sample, they also will lose smaller amounts of energy to the target electrons. As in Rutherford Backscattering (RBS), this will lead to depth sensitivity, provided that the backscattered ion energies are measured with sufficient resolution. The projectile ions are usually light—protons, alpha particles, or Li ions. In channeling, the incidence direction of the ion beam is fixed, and is aligned with a high symmetry direction of the substrate. In blocking,

the angular distribution (as well as the energy distribution) of the backscattered flux is measured. This angular distribution is characterized by minima, whose positions are closely connected to the relative positions of atoms in the surface layer. The experiments are performed at high angular and energy resolution. The latter fact also makes it possible to perform very high resolution depth profiling (even on a layer-by-layer basis), an application that in coming years will find increased use in materials science. MEIS differs from low-energy ion scattering (ISS) in that the interaction law in the latter is much more complex and difficult to understand, and because ISS is essentially sensitive only to the top layer. Compared to high-energy ion scattering (conventional RBS), MEIS is more surface sensitive, and more complex instrumentally. The high depth resolution of the atomic composition in MEIS (resulting from the type of ion detector that is used) is useful for studies of all solids (crystalline, noncrystalline, metallic, semiconducting, and insulating), while the specific application of channeling and blocking is applicable only to single-crystal samples, and is used to extract highly accurate values for the structural parameters (atomic positions) of surfaces and interfaces. To date, the technique has been applied mainly to the study of metals, semiconductors, and overlayers on such surfaces (submonolayer adsorbate concentrations, thin films of silicides, etc.), but recently it has been applied to insulators as well.

The basic ideas behind channeling and blocking can be understood from Figure 1. A well collimated beam of ions is incident along a high symmetry (channeling) direction of the target (a single crystal). Most of the incident ions will propagate in the large channels between the nuclei, where they will lose energy quasicontinuously to the electrons in the target. These energy losses will be on the order of tens of eV and will be frequent, but will not lead to large angular deviations because of the enormous mismatch of the ion-electron masses. A few ions will collide with the first atom along a row of target nuclei. The energy loss is such a collision may be large (≥ 1 keV) and a large angular deflection may also result. The angular distribution of the backscattered flux from the atoms in the first layer will be smooth. Due to geometrical distortions in the surface (contractions, reconstructions, etc.) or thermal vibrations, there may be a finite collision probability for deeper layers also. On their way back to the detector, electrons from the deeper layers cannot penetrate ions in layers closer to the surface. This means that the backscattered flux will be reduced in directions corresponding to a vector joining two atoms in different layers, and that the angular distributions will be marked with pronounced blocking dips, which contain direct information about the relative position of atoms in the first few layers of the crystal. Usually, the energy resolution of an experiment is not good enough to resolve the contributions from the different layers in the crystal, and the leading peak of the energy distribution (the surface peak) will contain contributions from several layers. The experimental parameters (the beam energy, the incidence direction, etc.) are usually set up such that the collision probabilities form a rapidly converging series; i.e., only three or four layers

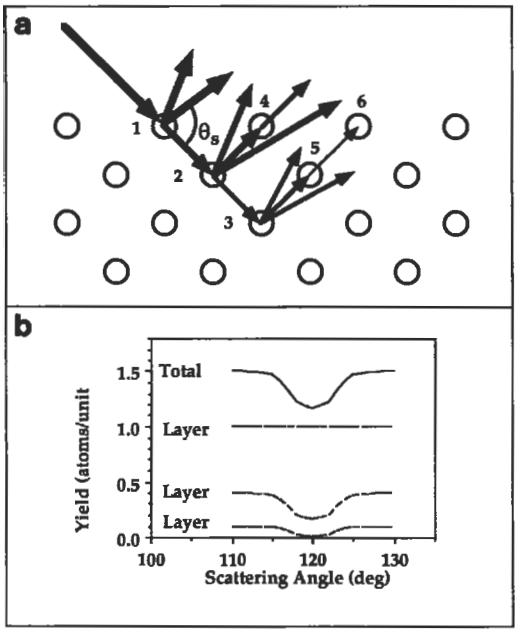

Figure 1 **Ion paths demonstrate MEIS and the effect of vibrations in a channeling and blocking experiment: (a) The widths of the arrows indicate the intensity of the ion flux at each point, and the atoms are numbered for reference to (b). (b) The angular distribution of the ions exiting the crystal, as well as the individual contributions from each layer of the crystal.**

contribute. The technique can also be used to study buried interfaces: One can easily separate the interface signal from the surface signal, say, for different lateral lattice parameters in the overlayer and the substrate (different channeling directions), and different atomic species at the interface can be distinguished through their signature backscattering energies.

We will review briefly the basic physics of ion scattering and will give a short overview of the experimental technology. We will conclude with some examples of the power of the technique. An exhaustive review of MEIS up to 1985 has been given by van der Veen; he covers both the basic principles and the results obtained.[1] More recently, Watson has made a comprehensive compilation of surface structural data obtained with MEIS and other ion scattering techniques.[2] More general introductions to ion scattering have been given by Feldman et al.[3, 4] The technique of medium-energy ion scattering originated at the FOM institute in Amsterdam, and the technical development is associated with the names of Frans Saris, Friso van der Veen, Ruud Tromp and their collaborators.

Basic Principles

Because of the high energy of the incident ions, the ion–target interaction is a series of binary events. The de Broglie wavelength of the ion is on the order of 10^{-3} Å, so that diffraction and other quantum mechanical effects are not important. By considering energy and momentum conservation, the energy loss in the collision may be calculated; it depends only upon scattering angle (θ_S) and the ratios of the ion and target masses ($\rho = m_1/m_2$). For an incident energy E_0 (and exit energy E_1) the fractional energy loss (or kinematic factor), K^2, is:

$$K^2 = \frac{E_1}{E_0} = \left[\frac{\rho\cos\theta_s + \sqrt{1-\rho^2\sin^2\theta_s}}{1+\rho}\right]^2 \tag{1}$$

The dependence on target mass makes ion scattering techniques ideal for the study of multielement systems. By increasing the incident ion mass, the energy separation between different elements becomes larger. On the other hand, radiation-induced damage becomes a more important consideration.

The amount of energy transferred to the target atom depends strongly upon the scattering angle and can be calculated directly from Equation (1). For a 100-keV beam, the energy losses are typically several keV. Such events will lead to sample damage. Due to the high velocity of the incident ions, the ion will have left the damaged region well before the recoiling target atom can cause any damage; damage avoidance therefore involves keeping the beam dose so low that the damaged region is not sampled by subsequent ions. This can be accomplished by efficient data collection (multidetection techniques), or by moving the ion beam to fresh spots on the sample and averaging the results. If the dose is not low enough beam damage, which leads to disorder, will become visible directly in the scattering spectra in the form of an increased background just behind the surface peak, and can be easily monitored in the spectra. The amount of damage has to be evaluated carefully in each experiment. Light substrates are more easily damaged than heavy ones. Many metals, fortunately, self anneal at room temperature, which facilitates analysis.

An important concept is the *shadow cone*, which is a region where no ions can penetrate due to the ion–nucleus repulsion (see Figure 2). This effect makes ion scattering surface sensitive. The size of the shadow cone R_s can be calculated for the classical Coulomb potential as:

$$R_s = \sqrt{\frac{4Z_1Z_2e^2d}{E}} \tag{2}$$

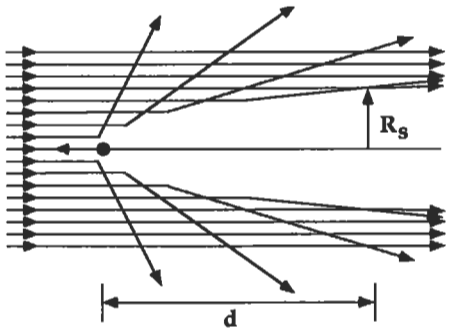

Figure 2 **Schematic of the shadow cone formed by the interaction of a parallel beam of ions with an atomic nucleus. For a static scatterer no ions can penetrate into the shadow cone.**

where R_s is measured a distance d behind the scattering center and Z_1 (Z_2) is the nuclear charge of the projectile (target atom). The shadow cone R_s is of a similar magnitude as a vibrational amplitude, and the visibility of the second layer atom will depend upon the ratio of these two numbers. In interpreting data, one also takes into account the fact that the surface vibrational amplitude is generally larger (by about a factor of 2) than the bulk amplitude, that it can be anisotropic, and that the vibrational amplitudes are correlated. Theoretical modeling of these effects rarely go beyond the Debye model.

The probability for a ion to scatter in a particular direction is determined by the ion–target interaction, and can be expressed in terms of a cross section σ_r. For a Coulomb potential, the differential cross section is the well-known Rutherford formula:

$$\sigma_r(\theta_s, E) = \left[\frac{Z_1 Z_2 e^2}{4E\sin^2\frac{\theta_s}{2}}\right]^2 g\left(\frac{M_1}{M_2}, \theta_s\right) \tag{3}$$

where $g(M_1/M_2, \theta_s)$ is due to the transformation from the center-of-mass frame to the lab frame, and is usually close to 1. Because the cross section is known on an absolute scale, one can predict the number of scattering events in a solid angle, given the number of incident ions. Conversely, one can invert this relationship and express the number of scattered ions in units of the number of atomic scatterers per surface unit cell. In practice, due to uncertainties in the exact angular acceptance and efficiency of the detector, as well as details due to the detector's geometry, one usually uses a calibrated standard, for example a known amount of Sb implanted in

a Si wafer. The measured ion yield also has to be corrected for the fact that some scattered ions are neutralized at the surface.(The ion fraction P+, as it is known, is typically 0.8–0.9, which is very different from the energy range used in ISS, where P+ can be as small as 0.01.) In this way, it is possible to study surfaces in absolute units; i.e., in the number of visible atoms per surface unit cell. This is a valuable feature of the technique. As we shall see, this allows us to discriminate between different structural models, based only on a simple inspection of the data.

To quantify the interpretation of ion scattering yields, one performs Monte Carlo simulations of the scattering process. In these simulations, the ion scattering experiment is performed numerically on a computer (a SUN Sparcstation or similar machine is adequate). Since the scattering cross section is known, the simulated yields may be compared directly to the experimental yields. Other than the obvious input of charges and masses of the ion and substrate atoms, the only inputs to the simulation are the positions and vibrational amplitudes of each of the atoms in the crystal. To find the correct structure, one must vary the relevant structural and vibrational parameters until an optimal fit is found. Fortunately, there is a large amount of intuitive information in the blocking dips. Therefore, it is possible to determined the sign, as well as an estimate of the magnitude of a structural rearrangement, without doing any simulations.

To measure the goodness of fit, and to quantify the structural determination, a reliability (*R*-factor) comparison is used. In comparing the data and simulation of the experiment for many trial structures, a minimum *R* factor can be found corresponding to the optimal structure. In this way atomic positions can be determined in favorable cases to within a few hundredths of an Å, comparable to the accuracy achieved in Low-Energy Electron Diffraction (LEED).

Instrumentation

At present there are fewer than 10 laboratories worldwide using channeling and blocking for surface structural work, while the number of groups with the technical capability of doing high-resolution depth profiling is perhaps a factor of 3 larger. All of the necessary equipment is available commercially, but most groups have preferred to custom build at least a portion of it. The main drawback of MEIS is that the instrumentation is expensive even by surface science standards, and this has limited the number of workers in the field. The use of a ~100-keV ion beam implies that a small ion accelerator is needed. An ultrahigh vacuum compatible sample manipulator is needed to position the specimen to within ~0.02° along three orthogonal axes. To measure the angular distribution of the ions, it is necessary to have a detector that measures both the energy and the scattering angle of the ions with high precision. Multidetection schemes are useful to minimize data accumulation times and beam-induced sample damage. The ion energy analysis is usually done by a commercially available toroidal high-resolution ion energy analyzer that

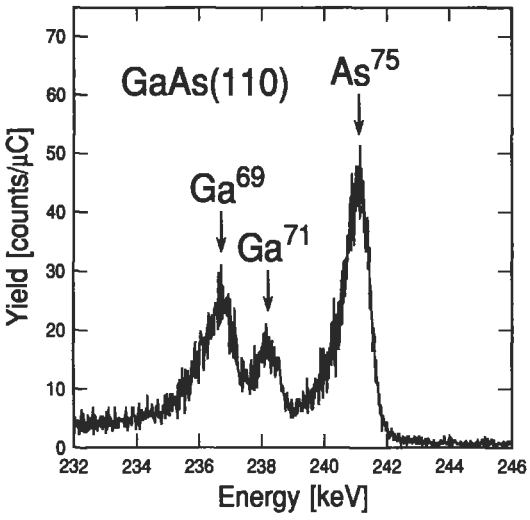

Figure 3 **Backscattering spectrum from GaAs (110), obtained with a 300-keV Li ion beam at a scattering angle of 85°.**

is free to move in the plane defined by the ion incidence direction and the surface normal. By determining the angular position at which the ion strikes the detector one recovers information about the angular distribution of the scattered ions; the radial position gives information about the energy. The energy resolution ΔE of the toroidal analyzer is determined primarily by the size of the beam spot on the sample and the size of the entrance slit. A total energy resolution (detector + ion beam width) ΔE of 150 eV at 100-keV primary energy is easily obtained. This is to be compared to the energy resolution of a conventional surface barrier detector (used in RBS), which can be ~10 keV at 1 MeV.

As an example, we show in Figure 3 a backscattering spectrum from GaAs (110), obtained with a 300-keV Li ion beam.[5] This is a well-chosen test example of energy resolution, as the atomic numbers of the two constituents are quite close (31 and 33 for Ga and As, respectively). Not only are these two species well resolved, but the two common isotopes of Ga are also well separated. Note that the peaks are asymmetric due to contributions from lower layers. Resolving power of this kind surely will find many new applications in materials science.

The main limitation to the accuracy of MEIS comes from systematic errors involving uncertainties in the vibrational modeling, the scattering cross section, and approximations in the ion scattering simulation code. All of these sources conspire to make a structural measurement of the complicated, highly distorted structures of heavy elements the most uncertain. On the other hand, the uncertainty in a measurement of the simple surface of a light element will approach 1% due to the angular resolution. It is difficult to estimate the magnitude of the systematic error

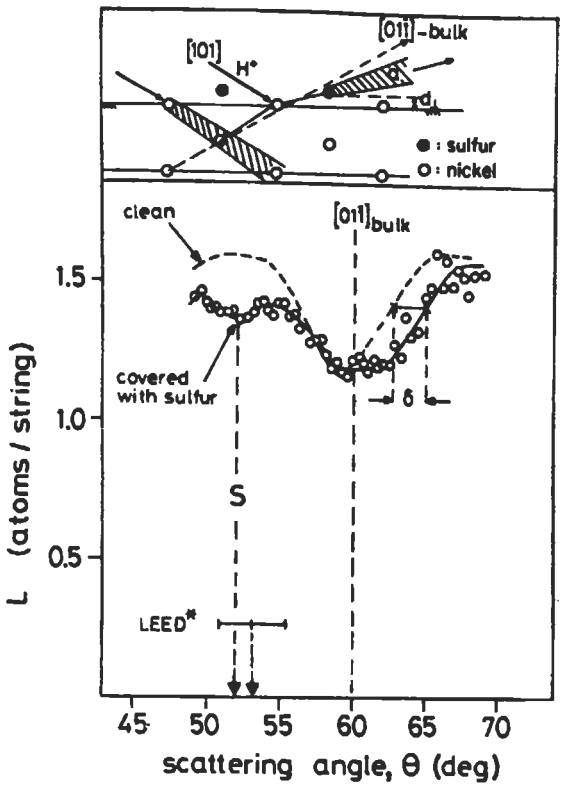

Figure 4 **Angular distribution of backscattered protons from clean and S-covered Ni(110). The top part of the figure shows the scattering geometry. The primary ion energy was 101 keV.**

in any given set of data. A typical MEIS experiment relies upon the analysis of many sets of data that overlap in sensitivity to a given structural parameter. The self-consistency of the analysis provides a direct measure of the magnitude of the systematic error. In several cases—for example, the (110) surfaces of Cu, Ni, Pt, Au, and III-V compound semiconductors like GaAs and InSb—both LEED and MEIS have been used to determine structural parameters with excellent mutual agreement and comparable accuracy.

Examples and Applications

We will illustrate the power of MEIS with three simple examples. In addition, we remind the reader of the existence of extensive reviews,[1, 2] and in particular would like to mention some quite recent, beautiful work on the melting of single-crystal surfaces.[6]

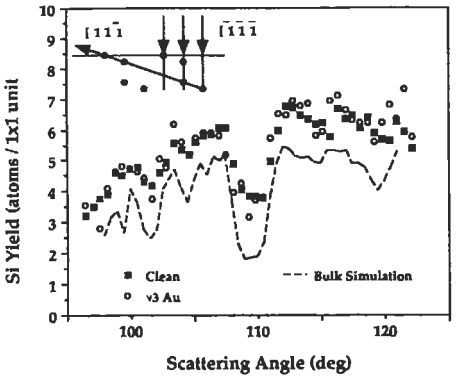

Figure 5 **Si backscattering yields (angular scans) for normal incidence on the Si (111) (7 × 7) surface (solid squares) and the Si (111) ($\sqrt{3} \times \sqrt{3}$) R30°-Au surface (open circles). The curve is the expected yield from a bulk terminated Si (111) surface. The scattering geometry is shown in the inset.**

S on Ni (110)

In Figure 4 we show MEIS data in the scattering geometry indicated for clean and sulphur-covered Ni (110).[7] For the clean surface, we observe a pronounced blocking dip at ~60°. The clean surface has a (1 × 1) LEED pattern, which means that the periodicity of the surface is that expected based on an extrapolation of the bulk geometry. However, the lattice spacing perpendicular to the surface may differ from that of the bulk. If the separation between the two outermost planes were unchanged, the blocking dip in Figure 4 would be observed at an angle of 60°. Clearly, the data are shifted towards smaller scattering angles, indicating a contraction of this spacing. By adsorbing 0.5 monolayers of sulphur on Ni (110), a (2 × 2) supercell is formed. The angular distribution of the Ni flux from this structure is also shown in the figure. One observes immediately that the dip is shifted to a larger scattering angle, indicating that the outermost Ni layer has now moved out past the bulk-like position and that the lattice is now expanded (a detailed numerical evaluation of the data show that the expansion is ~6%). In addition, a slight blocking dip is now observed around 53°. This dip corresponds to blocking of the outgoing Ni flux by the sulphur adatoms. The small size of this dip is due to the low concentration of the sulphur atoms and the fact that the light sulphur atoms are less efficient blockers than the heavier Ni atoms. The position of the dip allows us to determine the height of the sulphur atoms over the substrate (0.87 ± 0.03 Å).

Si (111) ($\sqrt{3} \times \sqrt{3}$) R30° Au

Gold is an example of a metal that does not form a silicide, and one may therefore expect the Au/Si interface to be abrupt. The $\sqrt{3}$ structures of Au on Si (111) are interesting in that the unit cell is much smaller than that of the well known (7 × 7)

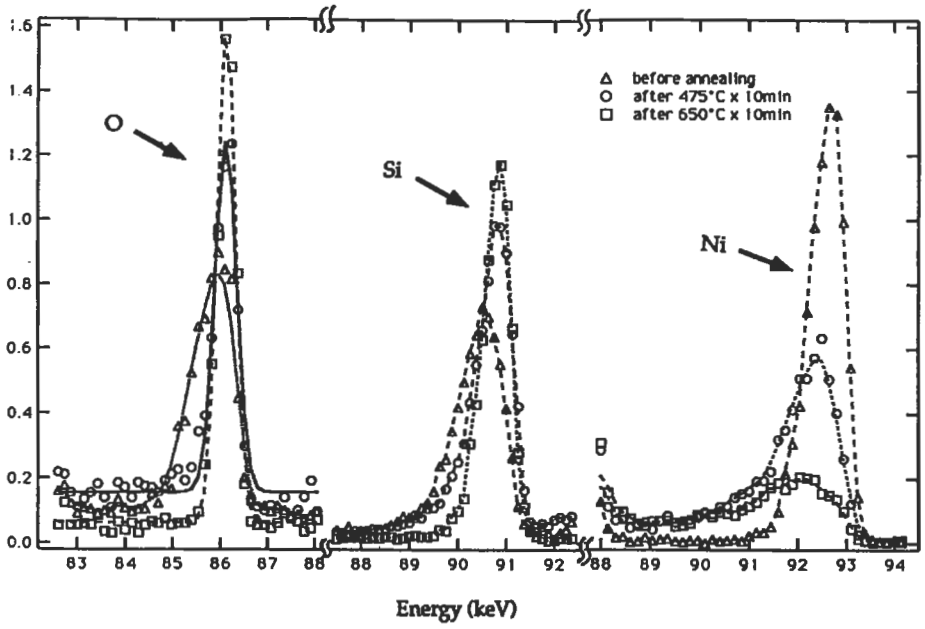

Figure 6 **Backscattering spectra for a thin film of Ni deposited on an amorphous SiO_2 film grown on top of Si (111) for three different annealing temperatures.**

structure of the clean surface. It might then seem plausible that this structure corresponds to a gentle modulation of an ideal (1×1) structure, with the Au atoms presumably close to Si lattice sites. Many drastically different models have been proposed for this structure; all are based implicitly on such assumptions. In Figure 5, we show MEIS data for the clean Si (111) (7×7) surface and for the $(\sqrt{3} \times \sqrt{3})$ R30° surface.[8] In addition, we show a computer simulation for what would be expected for an ideally terminated Si (111) (1×1) surface. Surprisingly, the two experimental spectra are rather similar and differ quite significantly from the calculated result. We find that Si atoms in more than one monolayer are displaced away from their lattice sites. The Au atoms do not block the outgoing Si flux. These conclusions, which are quite model independent, show that the Si lattice is severely distorted and that the Au atoms do not sit in Si lattice sites. The conclusions provide useful general constraints that more detailed models must obey. A more detailed analysis, based on Monte Carlo simulations for different trial structures, is necessary to establish a detailed structure. This shows that the structure most likely involves three Au atoms per unit cell, arranged in a trimer on a Si substrate, where the top half of the Si double layer is missing.

Ni/ SiO_2/ Si (111)

In Figure 6, we show MEIS energy spectra (for a fixed collection direction) for a thin film (initially some 6 monolayers) of Ni, deposited on top a thin film of SiO_2 grown on Si (111). As the three different atoms involved have widely differing masses, the signals from the three species are well resolved. The area under each peak is proportional to the concentration of each species. From the Ni peak, one can see that as the sample is annealed, the Ni starts diffusing into the bulk (the peak gets more and more asymmetric). The total concentration in the near surface region also decreases; evidently the diffusion into the bulk is quite rapid. The leading part of the Si peak falls initially at the energy of the clean Si (111) surface; the implication is that the surface is not completely covered by Ni, but that bare patches of SiO_2 remain. After annealing, the Si peak and the O peak move towards higher energies; this is consistent with less and less of the surface being covered by metal.

Conclusions

MEIS has proven to be a powerful and intuitive tool for the study of the composition and geometrical structure of surfaces and interfaces several layers below a surface. The fact that the technique is truly quantitative is all but unique in surface science. The use of very high resolution depth profiling, made possible by the high-resolution energy detectors in MEIS, will find increased applicability in many areas of materials science. With continued technical development, resulting in less costly instrumentation, the technique should become of even wider importance in the years to come.

This work was supported in part by National Science Foundation (NSF) Grant No. DMR-90-19868.

Related Articles in the Encyclopedia

RBS and ISS

References

1 J. F. van der Veen. *Surf. Sci. Rep.* **5,** 199, 1985. Basic principles of MEIS, with many results of structure determinations.

2 P. R. Watson. *J. Phys. Chem. Ref. Data.* **19,** 85, 1990. Compilation of structural data attained by MEIS and other ion scattering techniques.

3 L. C. Feldman, J. W. Mayer, and S. T. Picraux. *Materials Analysis by Ion Channeling.* Academic, New York, 1982. General introduction to ion scattering.

4 L. C. Feldman. *Crit. Rev. Solid State and Mat. Sci.* **10,** 143, 1981.

5 M. Copel and R. M. Tromp. Private communication.

6 J. F. van der Veen, B. Pluis, and A. W. van der Gon. In: *Chemistry and Physics of Solid Surfaces VII, Springer Series in Surface Sciences, Volume 10.* (R. Vanselow and R. F. Howe, eds.) Springer, Heidelberg, 1988, p. 455 and references therein.

7 J. F. van der Veen, R. M. Tromp, R. G. Smeenk, and F. Saris. *Surface Sci.* **82,** 468, 1979.

8 M. Chester and T. Gustafsson. *Phys. Rev. B.* **42,** 9233, 1990.

9.4 ISS

Ion Scattering Spectroscopy

GENE R. SPARROW

Contents

- Introduction
- Basic Principles
- Quantitation
- Advantages and Disadvantages
- Applications
- Conclusions

Introduction

Ion Scattering Spectroscopy (ISS) is one of the most powerful and practical methods of surface analysis available. However, it is underutilized due to a lack of understanding about its application and capabilities. This stems from its history, the limited number of high-performance instruments manufactured, and the small number of experienced surface scientists who have actually used ISS in extensive applications. Ironically, it is one of the easiest and most convenient surface analytical instruments to use and it provides useful information for almost any type of solid material.

The most useful application of ISS is in the detection and identification of surface contamination, which is one of the major causes of product failures and problems in product development. The surface composition of a solid material is almost always different than its bulk. Therefore, surface chemistry is usually the study of unknown surfaces of solid materials. To better understand the concept of "surface analysis," which is used very loosely among many scientists, we must first establish a definition for that term. This is particularly important when considering ISS

because of its extreme sensitivity to the surface. In most applications *surface analysis* implies the analysis of a finite thickness or depth of the outermost layers of a material, generally from the outer few atomic layers to a depth of 100–200 Å. Techniques encompassing layers greater than that are better described as thin-film analyses, or as depth profiles directed at obtaining other information. Techniques like Energy-Dispersive X-Ray Spectroscopy (EDS) and FTIR with ATR (Attenuated Total Reflection) generally do not fit the description of surface analysis. Other techniques, such as Auger and ESCA, meet the definition by obtaining spectra that originate from a depth of up to approximately 50–80 Å.

ISS is the most surface sensitive technique known. It is routinely sensitive to the outermost layer of atoms. At this level of depth sensitivity, it can be shown by ISS that most practical solid materials have the same outer atomic layer, i.e., a layer of surface water molecules, or organic material, with the hydrogen oriented upward. Therefore in ISS, as in SIMS using low-energy ions, it is important to include spectra from several different sputtered depths into the surface or to specify the sputtered depth from which the spectrum was obtained. Usually a series of ISS spectra are obtained at successively greater depths into the surface and the resulting spectra are displayed to show the changing composition versus depth. Because of the extreme surface sensitivity of ISS, these depth profiles offer details about changes in surface composition in the outer 50 Å that are generally not obtainable by other techniques. These details are extremely important in many applications, such as the initiation of corrosion, adhesion, bonding, thin-film coatings, lubrication, and electrical contact resistance. Typical data and applications will be discussed.

History

Earlier studies of ion scattering were directed primarily at gas–ion interactions. As studies of ion–solid surfaces became common the energy of the scattered ions was eventually related mathematically to a simple binary elastic event involving a single atom on a surface element and a single probe ion.

The practical use of ion scattering was not developed until the late 1960s when David P. Smith of 3M Company first reported the use of low-energy inert ion scattering to analyze the composition of surfaces. This early pioneering work established ion scattering as a very useful and viable spectroscopy for studying surfaces. The first studies and instruments consisted of simple systems where the ion beam scattered through an angle of 90°; thus accepting only a small solid angle of the signal. Modern systems use ion beams that are coaxial with the detector and exhibit orders of magnitude higher sensitivity. These devices make use of a Cylindrical Mirror Analyzer (CMA) and include detection of ions scattered about a 360° solid angle. A typical device is shown in Figure 1. ISS has since become readily available commercially and is recognized as one of the four major surface techniques, generally including ESCA (XPS), Auger, and SIMS as well.

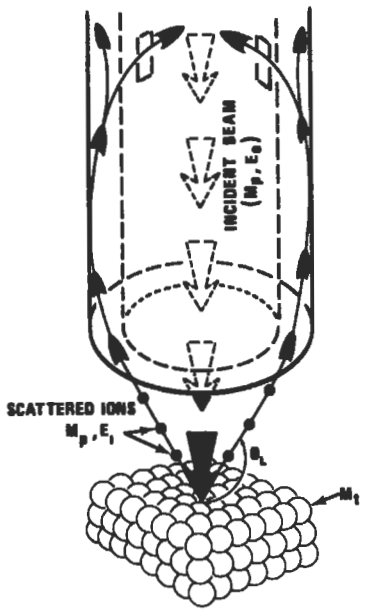

Figure 1 **Schematic of CMA ISS device showing primary ion beam, analyzer, and scattering at 138°.**

Basic Principles

ISS is relatively simple in principle and application. When a low-energy (100–5000 eV) beam of positive ions of some inert element, such as He, Ne, or Ar, strikes a surface, some of the ions are reflected back from the surface. This scattering process involves a single surface atom and a single incident ion. It is, therefore, a simple binary elastic collision that follows all the rules of classical physics. The incident ion scatters back with a loss of energy that depends only on the mass of the surface atom (element) with which the collision occurred. The heavier the surface atom, the smaller the change in energy of the scattered ion. Thus carbon, which is a light atom of mass 12, is readily displaced and the probe ion loses most of its energy, whereas a heavy atom like Pb, having mass 208, is not easily moved. An ion scattering from Pb retains most of its incoming energy. To obtain a spectrum, one merely records the number of scattered ions as their energy is scanned from near 0 eV to the energy of the primary incoming beam. Each element has a unique mass and therefore a unique energy at which the probe ion scatters. The energy of the scattered ion is mathematically related to the mass of the surface atom by the following equation:

$$\frac{E_1}{E_0} = E_r = \frac{M_1^2}{(M_1 + M_2)^2}\left(\cos\theta + \sqrt{\left(\frac{M_2}{M_1}\right)^2 - (\sin\theta)^2}\right)^2$$

where E_0 is the energy of the incident probe ion, E_1 is the energy of the ion scattered from surface atom, E_r is the ratio of the energies of the scattered and probe ions, M_1 is the mass of the primary ion, M_2 is the mass of the surface atom, and θ is the scattering angle measured from the direction of the ion beam.

Penetration of the incident beam below the very outermost atomic layer causes excessive and nondiscrete loss of energy such that the scattered ions do not yield sharp, discrete peaks. Only ions scattered from the outer atomic layer of a surface give rise to a sharp peak. ISS is therefore extremely sensitive to the surface and essentially detects only the outermost surface layer. To obtain more extensive surface information, it is therefore common to continuously monitor the ISS spectrum while sputtering into the surface. When the sputtering is done very slowly using a light atom, such as isotopically pure $^3He^+$, complete spectra can be obtained at successively greater depths into the surface. In routine practice, sputter rates on the order of about 1 to 5 Å per minute are used and approximately 15–20 ISS spectra are obtained throughout a sputtered depth of about 100 Å. Since the most important information is obtained near the surface, the majority of these spectra are obtained in the first few minutes of sputtering.

As the scattering angle θ is decreased to 90°, the physical size of the CMA must increase, until finally one cannot use a CMA but must resort to a sector analyzer. This decreases detection sensitivity by 2–3 orders of magnitude, increases multiple scattering at energies above the primary peaks, and requires much more precise positioning of the sample. Changing the mass of the primary ion beam gas controls not only the sputtering rate of the surface but also changes the spectral resolution and detection sensitivity. For example, using $^3He^+$ permits good detection of C, N, and O, whereas using $^4He^+$ does not. Using Ar^+ provides high sputtering rates for deeper profiles but does not permit the detection of elements having mass less than Ca. Argon also provides increased spectral resolution for higher elements not resolved by He. It is common to sometimes mix Ar and He to detect all elements while obtaining a high sputtering rate. Increasing the energy of the primary beam to above about 3000 eV dramatically increases the overall spectral background, thus decreasing sensitivity, but the spectral resolution increases. Decreasing the beam energy decreases this background and dramatically decreases the sputtering rate. It is possible to obtain useful ISS spectra at energies below 200 eV of He at less than a few nA. The sputtering rate under these conditions is extremely low.

During normal operation, the entire ISS spectrum, covering all elements, is scanned in about 1 second. A number of these scans are then added for signal enhancement and to control the predetermined depth to which sputtering is

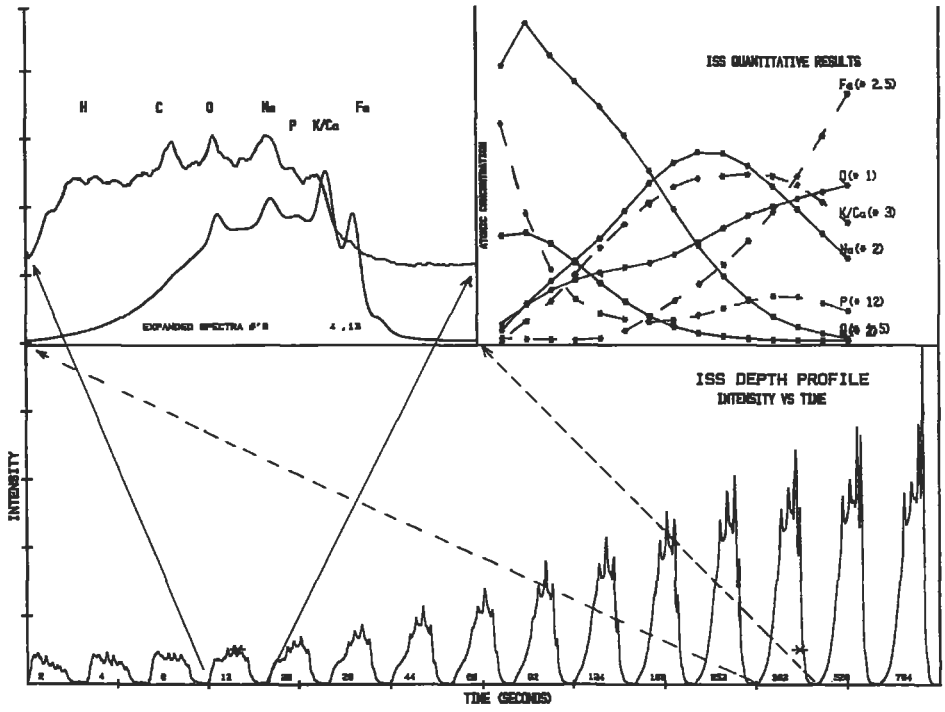

Figure 2 **Typical ISS spectral data obtained from routine depth profile of cleaned washed steel. Left spectrum represents surface. Right spectrum represents about 50-Å depth. Expansions shown top left. Relative atomic compositions plotted top right.**

desired. Since the greatest amount of surface information is usually obtained from the outermost layer, the initial spectra are obtained by restricting the accumulations to only 2 scans. At greater depths, many scans may be averaged to obtain one spectrum. When all of these spectra are normalized and plotted on a single figure, a depth profile is obtained that illustrates in great detail how the surface composition changes with depth. Figure 2 illustrates typical data obtained from such a plot. The spectrum on the extreme bottom left illustrates the composition at the outermost surface, whereas the spectrum on the extreme bottom right illustrates composition after sputtering to about 50 Å. In general, many of the compositional changes observed in the first few spectra are not detected in either AES or ESCA. In this particular sample, for example, changes in C, O, and Fe were detected in Auger profiles when sputtering to about 30 Å, but Ca was detected only in trace levels and H, Na, P, and Ba were not detected. The concentration of Fe at the surface was shown to be about 28% by AES (within the finite depth probed), whereas ISS (the first trace) clearly shows Fe is completely covered by contaminants. In the same figure, two spectra (numbers 4 and 13 in the profiled series) have been expanded in the

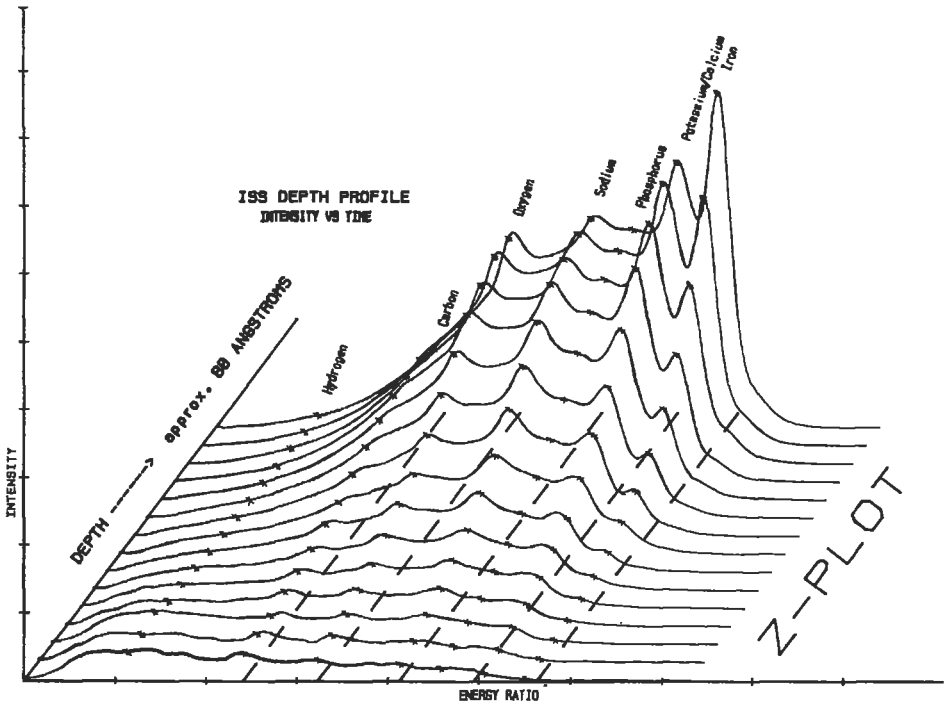

Figure 3 ***Z*-plot of ISS data shown in Figure 2. Each spectrum represents the composition of the surface at a different cross section in depth.**

upper lefthand corner to show the changes in detail, and actual atomic concentrations of the elements detected are shown in the upper righthand plot.

When all of the ISS spectra are plotted in a three-dimensional manner, such as the "*z*- plot" shown in Figure 3, the changes in surface composition with depth are much more obvious. In this figure, each spectrum represents the composition at a different cross section of the total depth sputtered, hence the spectra are plotted at different depths. Note that the spectra are not recorded at identical incremental depths.

Quantitation

ISS involves simple principles of classical physics and is one of the simplest spectroscopy for quantitative calculations. Under most standard instrumental operating conditions there is essentially no dependency on the chemical bonding or matrix of the sample. Several workers[1–6] have discussed quantitative aspects of ISS and elemental relative sensitivities. These have been compiled[7] with comparative measurements of sensitivity obtained from several different laboratories and are shown in

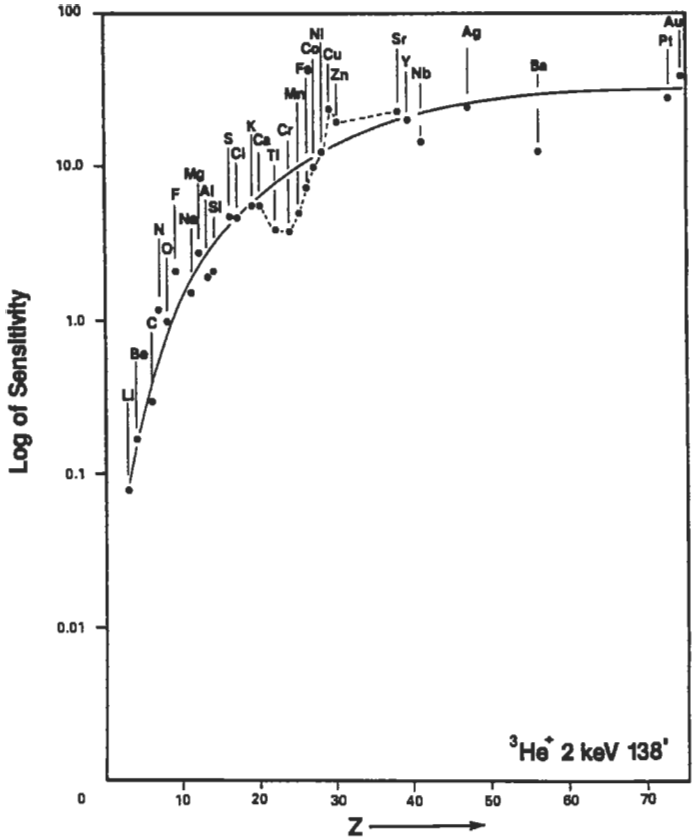

Figure 4 **Relative elemental sensitivities for ISS scattering using $^3He^+$ at 2000 eV.**

Figure 4 for $^3He^+$ scattering. In general, the precision of ISS is extremely high under routine conditions and can approach well under 1% relative for many measurements. When used with appropriate standards, it can provide very accurate results. This makes it extremely useful for comparisons of metal and oxygen levels, for example.

Several features of ISS quantitative analysis should be noted. First of all, the relative sensitivities for the elements increase monotonically with mass. Essentially none of the other surface spectroscopies exhibit this simplicity. Because of this simple relationship, it is possible to mathematically manipulate the entire ISS spectrum such that the signal intensity is a direct quantitative representation of the surface. This is illustrated in Figure 5, which shows a depth profile of clean electrical connector pins. Atomic concentration can be read roughly as atomic percent directly from the approximate scale at the left.

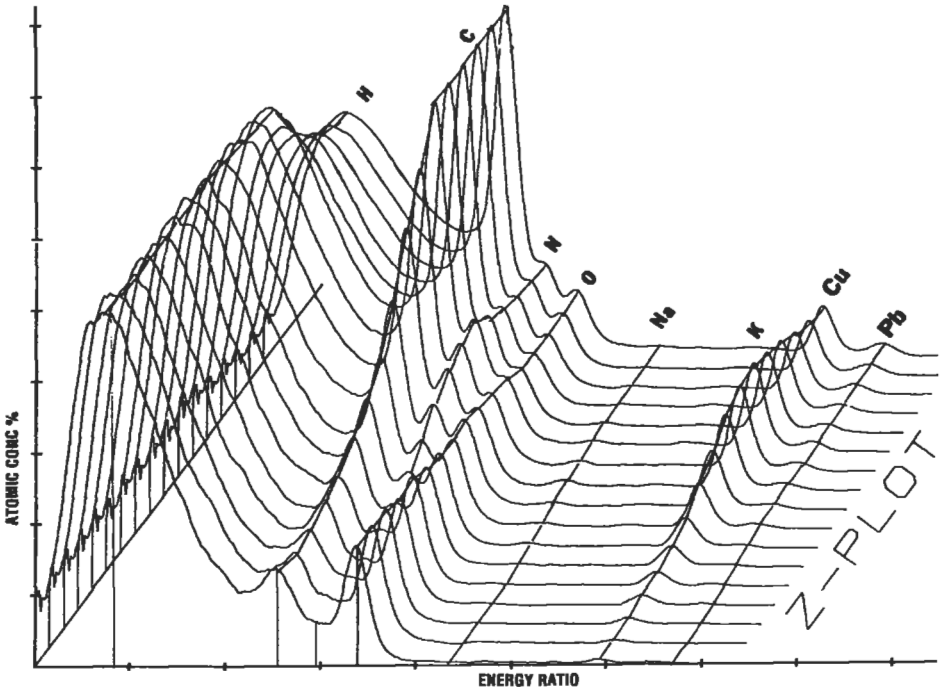

Figure 5 ***Z*-plot of polyamide delaminated from Cu metal film. Entire spectra have been mathematically treated to adjust for detector response versus energy. Each spectrum represents the composition at a different depth. Peak height can be read roughly as atomic concentrations at left.**

In addition to its precision and simplicity, ISS is also the only technique that can be used for quantitative analysis of hydrogen within the outer surface of material. Although SIMS can detect hydrogen, it is extremely difficult to quantitate it on the outer surface. Unlike detection of all other elements, the detection of hydrogen in ISS does not involve scattering from hydrogen but rather the detection of sputtered hydrogen, which passes through the detector and is detected at low energies in the spectrum. Through use of appropriate references, such as polymers, quantitative analysis has become possible. Even extremely small changes in hydrogen content, such as from differences in adsorbed water, are detectable. This makes ISS extremely valuable for the analysis of polymer surfaces.

There are two major drawbacks to ISS concerning quantitative analysis. First, it has very low spectral resolution. Thus it is very difficult either to identify or resolve many common adjacent elements, such as Al/SI, K/Ca, and Cu/Zn. If the elements of interest are sufficiently high in mass, this can be partially controlled by using a probe gas with a higher atomic mass, such as Ne or Ar. Second, ISS has an inherently high spectral background which often makes it difficult to determine

true peak intensity. However, modern computer techniques provide significant ways to minimize these problems and quantitative results are obtained routinely. The relative detection sensitivity of ISS varies considerably depending on the type of sample and its composition. In general, the sensitivity can be as good as 20–50 ppm for a high-mass component, such as Pb in a low-mass substrate like Si, or as poor as a few percent, such as for C in a low-mass substrate like Al.

Advantages and Disadvantages

The most important features of ISS are its extreme speed—less than 0.5 s to obtain a single spectrum—and its extreme sensitivity to the outer surface. The speed is directly related to the high detection sensitivity of ISS, which can be well in excess of 10,000 counts of signal per nA (cps/nA) of ion beam signal for Ag. Other important features of ISS are that it is extremely simple in principle, operation, and instrumentation. The data presentation are extremely simple, exhibiting little noise and high precision and reproducibility. It is easily applied to nearly any material and is especially useful for the analysis of polymers or interfacial failures. ISS is normally very cost-effective, with pricing of instruments being very low and instrument size being small. Experimental set-up, data collection, and data manipulation are relatively simple.

Extreme sensitivity to the outer surface is the most useful advantage of ISS. It is unexcelled in this respect and has the unique capability to detect only the outermost atomic layer without signal dilution from many additional underlying layers. No other technique, including static SIMS or angle-resolved XPS, can detect only the outermost atomic layer. ISS is also very fast and sensitive, so that even very low level impurities within the outer few Å can be detected. Other very important advantages are the speed of depth profiling and the extreme detail one can obtain about the changes in chemical composition within the outer surface, especially the first 50–100 Å (i.e., the high depth resolution owing to sensitivity to the first atomic layer). The indirect detection of hydrogen also has proven extremely applicable to studies of polymers and other materials containing surface hydrogen in any form. This has been especially valuable in applications involving plasmas and corona treatments of polymers. ISS is routinely applicable to the analysis of insulators and irregularly shaped samples. In some research and development applications its ability to detect certain isotopes, such as O^{18}, are especially important. Quantitative analysis is also advantageous, since ISS does not miss elements that are often overlooked in other spectroscopies due to poor sensitivity (such as H, the alkalis, and the noble metals), and quantitative calculations are not affected by the matrix. In addition these relative sensitivities do not vary as dramatically as in some other spectroscopies and they are uniformly increasing with the mass of the elements.

One of the major disadvantages of ISS is its low spatial resolution. In most of the current systems, this is limited to about 120 μm because of limits on ion-beam

diameter, although some work has been reported on ISS using an ion-beam diameter of about 5 μm. However, as the ion-beam diameter decreases, its energy normally increases, and this results in undesirable increases in the overall background of the spectrum. Another serious disadvantage of ISS is its low spectral resolution. Usually, this resolution is limited to about 4–5% of the mass of the detected element; hence it is very difficult to resolve unequivocally adjacent elements, especially at high mass. Although the spectral resolution can be improved to about 2% with instrument modifications or by computer deconvolution, this problem cannot be totally resolved. ISS also does not provide any information concerning the nature of chemical bonding, although a special technique called Resonance Charge Exchange (RCE)[8, 9] offers information about some elements. Ironically, the extreme surface sensitivity of ISS can become a disadvantage due to the "moving front" along which depth profiling can occur. For example, heavy surface atoms often are retained along this outer atomic layer during sputtering and are thus detected at levels far above what is representative of deeper layers in a thick film. Another key disadvantage is the technique's low sensitivity to certain important elements, such as N, P, S, and Cl, which are often more easily detected by AES or ESCA.

Typical Applications

Polymers and Adhesives

Applications of ISS to polymer analysis can provide some extremely useful and unique information that cannot be obtained by other means. This makes it extremely complementary to use ISS with other techniques, such as XPS and static SIMS. Some particularly important applications include the analysis of oxidation or degradation of polymers, adhesive failures, delaminations, silicone contamination, discolorations, and contamination by both organic or inorganic materials within the very outer layers of a sample. XPS and static SIMS are extremely complementary when used in these studies, although these contaminants often are undetected by XPS and too complex because of interferences in SIMS. The concentration, and especially the thickness, of these thin surface layers has been found to have profound affects on adhesion. Besides problems in adhesion, ISS has proven very useful in studies related to printing operations, which are extremely sensitive to surface chemistry in the very outer layers.

Metals

Perhaps the most useful application of ISS stems from its ability to monitor very precisely the concentration and thickness of contaminants on metals during development of optimum processing and cleaning operations. One particularly important application involves quantitatively monitoring total carbon on cleaned steels before paint coating. This has been useful in helping to develop optimum bond

strength, as well as improved corrosion resistance. Other very common applications of ISS to metals include the detection of undesirable contaminants on electrical contacts or leads and accurate measurements of their oxide thickness. These factors can lead to disbonding, corrosion, tarnish, poor solderability, and electronic switch failures.

Ceramics

Two capabilities of ISS are important in applications to the analysis of ceramics. One of these is its surface sensitivity. Many catalyst systems use ceramics where the surface chemistry of the outer 50 Å or less is extremely important to performance. Comparing the ratio of H and O to Al or Si is equally important for many systems involving bonding operations, such as ceramic detectors, thin films, and hydroxyapatite for medical purposes.

Conclusions

ISS is too frequently thought of as being useful only for the analysis of the outer atomic layer. It is a powerful technique that should be considered strongly for nearly any application involving surface analysis. It is easy to use and displays results about the details of surface composition in a very simple, quantitative manner. It is relatively quick and inexpensive and extremely sensitive to changes and contamination in the outer surface, which is not as readily investigated by AES or ESCA. It has very high sensitivity to metals, especially in polymers or ceramics, and is applicable to virtually any solid, although its poor spectral resolution often make it difficult to distinguish adjacent masses. Future trends will most likely result in making ISS much more common than it presently is and instrumental developments will most likely include much improved spectral resolution and spatial resolution, as well as sensitivity. Computer software improvements will increase its speed and precision even further, and incorporate such things as peak deconvolution, database management, and sputtering rate corrections. Commercial instruments and analytical testing with excellent computer software and interfacing are readily available. As with all techniques, ISS is best used in conjunction with another technique, especially SIMS or ESCA. Further reading on the principles of ISS and some applications can be found in references 10 and 11.

Related Articles in the Encyclopedia

SIMS, XPS, AES, and RBS

References

1 H. Niehus and E. Bauer. *Surface Sci.* **47**, 222, 1975.

2 E. Tagluner and W. Heiland. *Surface Sci.* **47**, 234, 1975.

3 H. H.Brongersma and T. M. Buck. *Nucl. Instr. Meth.* **132,** 559, 1976.

4 M. A. Wheeler. *Anal. Chem.* **47,** 146, 1975.

5 E. N. Haussler. *Surf. Interface Anal.* 1979.

6 G. C. Nelson. *Anal. Chem.* **46,** (13) 2046, 1974.

7 G. R. Sparrow. *Relative Sensitivities for ISS.* Available from Advanced R & D, 245 E. 6th St., St. Paul, MN 55010.

8 T. W. Rusch and R. L. Erickson. Energy Dependence of Scattered Ion Yields in ISS. *J. Vac. Sci. Technol.* **13,** 374, 1976.

9 D. L. Christensen, V. G. Mossoti, T. W. Rusch, and R. L. Erickson. *Chem. Phys. Lett.* **44,** 8, 1976.

10 W. Heiland. *Electron Fisc. Applic.* 17, 1974. Covers further basic principles of ISS.

11 D.P. Smith. *Surface Sci.* **25**, 171, 1971.